



It is estimated to average 1 hour per response, including the time for reviewing instructions, searching existing data sources, gathering and reviewing the collection of information, sending comments regarding this burden estimate or any other aspect of this collection of information, to Washington Headquarters Services, Directorate for Information Operations and Reports, 1215 Jefferson Avenue, Washington, DC 20540, and to the Office of Management and Budget, Paperwork Reduction Project (0704-0188), Washington, DC 20503.

2. REPORT DATE July 8, 1994		3. REPORT TYPE AND DATES COVERED Technical Report #2	
4. TITLE AND SUBTITLE Photogeneration of Charge Carriers in Bilayer Assemblies of Conjugated Rigid-Rod Polymers		5. FUNDING NUMBERS N00014-94-1-0540 Kenneth J. Wynne R & T Code: 3132111	
6. AUTHOR(S) J.A. Osaheni, S.A. Jenekhe, and J. Perlstein		7. PERFORMING ORGANIZATION NAME(S) AND ADDRESS(ES) Department of Chemical Engineering University of Rochester 206 Gavett Hall Rochester, NY 14627-0166	
8. PERFORMING ORGANIZATION REPORT NUMBER #2		9. SPONSORING/MONITORING AGENCY NAME(S) AND ADDRESS(ES) Office of Naval Research 800 North Quincy Street Arlington, VA 22217-5000	
10. SPONSORING/MONITORING AGENCY REPORT NUMBER		11. SUPPLEMENTARY NOTES Prepared for publication in <u>Journal of Physical Chemistry</u>	
12a. DISTRIBUTION/AVAILABILITY STATEMENT Reproduction in whole or in part is permitted for any purpose of the United States Government. This document has been approved for public release and sale; its distribution is unlimited.		12b. DISTRIBUTION CODE	
13. ABSTRACT (Maximum 200 words) <p>The quantum yield and the mechanism of photogeneration of charge carriers are investigated in bilayer assemblies consisting of a π-conjugated rigid-rod polymer layer and a triarylamine doped polycarbonate layer. The electric field dependent quantum efficiency of photocarrier generation, $\phi(E)$, in the bilayers containing a series of conjugated polybenzobisazoles was measured by photoinduced discharge and was found to be in the range of 10^{-3} to 10^{-2} at low fields ($<10^4$ V/cm) and as high as 0.12 - 0.32 at $\sim 10^6$ V/cm. The $\phi(E)$ data were qualitatively in accord with Onsager's three-dimensional model for ion-pair dissociation. Transient (ps) absorption spectroscopy of single layer thin films of the polymers showed that the primary photoexcitations were excitons. However, picosecond photoinduced absorption and photoluminescence experiments on the bilayers revealed photoinduced electron transfer and exciplex formation at the bilayer interface. Thus photocarrier generation on photoexcitation of the conjugated rigid-rod polymers in the bilayer occurs by photoinduced electron transfer, forming intermolecular exciplexes which dissociate efficiently in electric field. This mechanistic picture of charge carrier photogeneration provided a satisfactory account for the observed field dependent quantum yields in the series of bilayer assemblies.</p>			
14. SUBJECT TERMS Charge photogeneration, photocarrier generation efficiency, mechanism of photogeneration, conjugated rigid-rod polymers, bilayer assemblies, electron transfer, exciplexes.		15. NUMBER OF PAGES 48	
16. PRICE CODE		17. SECURITY CLASSIFICATION OF REPORT Unclassified	
18. SECURITY CLASSIFICATION OF THIS PAGE Unclassified		19. SECURITY CLASSIFICATION OF ABSTRACT Unclassified	
20. LIMITATION OF ABSTRACT Unlimited			

OFFICE OF NAVAL RESEARCH

GRANT N00014-94-1-0540

R&T Code 3132111

Kenneth J. Wynne

Technical Report No. 2

Photogeneration of Charge Carriers in Bilayer Assemblies
of Conjugated Rigid-Rod Polymers

by

John A. Osaheni, Samson A. Jenekhe and Jerry Perlstein

Prepared for Publication

in the

Journal of Physical Chemistry

University of Rochester
Department of Chemical Engineering
Rochester, NY

July 8, 1994

Reproduction in whole or in part is permitted for any purpose of the United
States Government

This document has been approved for public release and sale;
its distribution is unlimited.

TECHNICAL REPORT DISTRIBUTION LIST - GENERAL

Office of Naval Research (1)*
Chemistry and Physics Division
Ballston Tower 1, Room 503
800 North Quincy Street
Arlington, Virginia 22217-5660

Dr. Richard W. Drisko (1)
Naval Civil Engineering
Laboratory
Code L52
Port Hueneme, CA 93043

Defense Technical Information Center (2)
Building 5, Cameron Station
Alexandria, VA 22314

Dr. Harold H. Singerman (1)
Naval Surface Warfare Center
Carderock Division Detachment
Annapolis, MD 21402-1198

Dr. James S. Murday (1)
Chemistry Division, Code 6100
Naval Research Laboratory
Washington, D.C. 20375-5000

Dr. Eugene C. Fischer (1)
Code 2840
Naval Surface Warfare Center
Carderock Division Detachment
Annapolis, MD 21402-1198

Dr. Kelvin Higa (1)
Chemistry Division, Code 385
Naval Air Weapons Center
Weapons Division
China Lake, CA 93555-6001

Dr. Bernard E. Douda (1)
Crane Division
Naval Surface Warfare Center
Crane, Indiana 47522-5000

Dr. Peter Seligman (1)
Naval Command, Control and
Ocean Surveillance Center
RDT&E Division
San Diego, CA 92152-5000

Accession For	
NTIS GRA&I	<input checked="" type="checkbox"/>
DTIC TAB	<input type="checkbox"/>
Unannounced	<input type="checkbox"/>
Justification	
By _____	
Distribution/_____	
Availability Codes	
Dist	Avail and/or Special
A-1	

* Number of copies to forward

Photogeneration of Charge Carriers in Bilayer Assemblies of Conjugated Rigid-Rod Polymers

John A. Osaheni and Samson A. Jenekhe*

*Department of Chemical Engineering and Center for Photoinduced Charge Transfer,
University of Rochester, Rochester, New York 14627-0166.*

Jerry Perlstein

*Center for Photoinduced Charge Transfer and Department of Chemistry,
University of Rochester, Rochester, New York 14627*

ABSTRACT

The quantum yield and the mechanism of photogeneration of charge carriers are investigated in bilayer assemblies consisting of a π -conjugated rigid-rod polymer layer and a triarylamine doped polycarbonate layer. The electric field dependent quantum efficiency of photocarrier generation, $\phi(E)$, in the bilayers containing a series of conjugated polybenzobisazoles was measured by photoinduced discharge and was found to be in the range of 10^{-3} to 10^{-2} at low fields ($<10^4$ V/cm) and as high as 0.12 - 0.32 at $\sim 10^6$ V/cm. The $\phi(E)$ data were qualitatively in accord with Onsager's three-dimensional model for ion-pair dissociation. Transient (ps) absorption spectroscopy of single layer thin films of the polymers showed that the primary photoexcitations were excitons. However, picosecond photoinduced absorption and photoluminescence experiments on the bilayers revealed photoinduced electron transfer and exciplex formation at the bilayer interface. Thus photocarrier generation on photoexcitation of the conjugated rigid-rod polymers in the bilayers occurs by photoinduced electron transfer, forming intermolecular exciplexes which dissociate efficiently in electric field. This mechanistic picture of charge carrier photogeneration provided a satisfactory account for the observed field dependent quantum yields in the series of bilayer assemblies.

* To whom correspondence should be addressed.

INTRODUCTION

Photoinduced processes in π -conjugated polymers, including photogeneration of charge carriers, transport of photocarriers, and photoinduced charge transfer, have been widely investigated.¹⁻²⁰ The fundamental understanding of these photoinduced processes is of interest for theoretical and experimental understanding of the electronic structure and photoelectronic properties of conjugated polymers and for the design and optimization of optoelectronic devices such as electroluminescent diodes²¹, photovoltaic cells²², and xerographic photoreceptors.¹⁷ A variety of experimental techniques such as steady-state and transient photoconductivity and transient photoinduced absorption have thus been employed to investigate photocarrier generation and transport in conjugated polymers.¹⁻²⁰ However, the nature of charge photogeneration and the related photophysical processes in conjugated polymers remain poorly understood.^{11,23}

Prior reports of photoconductivity or charge photogeneration in conjugated polymers include studies on polydiacetylenes^{3,6}, polyacetylene^{1,2}, poly(3-alkylthiophenes)⁷, poly(*p*-phenylene vinylene)^{4,5} and polyquinolines.⁸ Two basic microscopic pictures have been advanced to rationalize the experimental observations on photocarrier generation in conjugated polymers. Based on spectroscopic and photoconductivity studies on polydiacetylenes and derivatives of poly(*p*-phenylene vinylene) (PPV), Bassler⁵ and others⁶ have proposed that photocarriers in these materials are produced by temperature- and field-assisted dissociation of photogenerated excitons in accord with Onsager's theory²⁴ of geminate ion-pair dissociation. Onsager's theory has similarly been applied successfully to describe photogeneration in molecular crystals^{25,26} and molecularly doped polymers (i.e. solid solutions of dye molecules in polymers).^{25,26} However, Moses et al.³ have challenged the applicability of Onsager's model to charge photogeneration in conjugated polymers, including polydiacetylenes and poly(3-

alkylthiophenes). These authors proposed instead the photogeneration of free carriers through interband transition, akin to free carrier production in semiconductors. Further studies on these and other conjugated polymers are thus needed to clarify the mechanistic picture of charge photogeneration in conjugated polymers.

The critical role of photoinduced electron transfer in the large enhancement of photoconductivity and corresponding quenching of photoluminescence in derivatives of PPV and polythiophene mixed with fullerenes (C_{60}) was recently reported.^{15,16} In such C_{60} /conjugated polymer mixtures, quantum yield for charge photogeneration is believed to approach unity due to efficient photoinduced charge transfer and charge separation. However, the quantum yield has not been measured.^{15,16} The direct measurement of the quantum efficiency for photoinduced charge transfer of holes and electrons from PPV to a donor triarylamine molecule and an acceptor (4-n-butoxycarbonyl-9-fluorenylidene) malononitrile has recently been reported from our laboratory.²⁰ The quantum yield was 0.25 and 2×10^{-3} for transfer of holes and electrons respectively from PPV.^{20b}

Our studies reported here were aimed at the determination of the electric field-dependent quantum efficiency of charge photogeneration and the mechanistic understanding of photocarrier generation in π -conjugated polymers. These studies were done primarily in *bilayer assemblies* consisting of a layer of a conjugated polymer and a layer of triarylamine dispersed in poly(bisphenol A carbonate) which is known to be a good electron donor that transports hole efficiently.^{25b} The field-dependent quantum efficiency $\phi(E)$ of charge carrier photogeneration in several conjugated polymers incorporated into the bilayers was measured by the xerographic photoinduced discharge technique.²⁶ The quantum yield measurements in conjunction with steady-state and picosecond-resolved photoluminescence and picosecond photoinduced absorption spectroscopies were used to explore the mechanism of photocarrier generation in the materials. It is shown that the high quantum efficiency ($\phi = 0.12 - 0.32$) of photocarrier generation in these polymers is due to efficient

electric field dissociation of *polymer/triarylamine exciplexes* formed by photoinduced electron transfer at the *bilayer interface*.

The π -conjugated polymers that we have selected for exploring charge photogeneration are the rigid-rod polybenzobisazoles shown in Chart I. These include poly(*p*-phenylene benzobisthiazole) (PBZT), poly(benzobisthiazole-4,4'-biphenylene) (PBBZT), poly(benzobisthiazole-1,4-phenylenebisvinylene) (PBTPV), poly(*p*-phenylene benzobisoxazole) (PBO), and poly(benzimidazobenzophenanthroline) ladder (BBL). Also shown in Chart I are the structures of the triarylamine donor molecules tris(*p*-tolyl)amine (TTA) and N,N'-diphenyl-N,N'-bis(3-methylphenyl)-4,4'-diamine (TPD) and the matrix polymer, poly(bisphenol A carbonate) (PC). The conjugated rigid-rod polybenzobisazoles have robust physical and chemical properties and are readily processable into high quality thin films and coatings.²⁷ We have previously reported the synthesis and characterization^{28,29} of these polymers and investigated their third-order nonlinear optical properties.³⁰⁻³² The use of PBZT as a charge generation layer in layered photoreceptors was reported in a communication.¹⁷ Initial studies of exciplex formation and exciplex luminescence of *bilayer assemblies* of these conjugated polymers with TTA have also been reported.^{18,23}

EXPERIMENTAL SECTION

Sample Preparation

The bilayer devices were prepared by spin coating isotropic solutions of the conjugated polymers onto 5x5 cm² poly(ethylene terephthalate) (PET) substrates overcoated with evaporated nickel which has an optical density of 0.4. The method of reversible Lewis acid coordination complexation²⁷ was used to prepare the isotropic solutions of the rigid-rod polymers in nitromethane containing aluminum chloride or gallium chloride (AlCl₃ or GaCl₃). The polymer/Lewis acid complex coating was washed

several times with deionized water and subsequently placed in a beaker of fresh deionized water overnight to ensure complete removal of the Lewis acid.²⁷ The resulting polymer thin films were dried in a vacuum oven for six hours at 80 °C. The polymer thin films which varied between 0.05-1 μm in thickness, were subsequently overcoated with a 15-20 μm layer of TTA/PC solid solution by using a blade coating technique. The TTA/PC layer was in the ratio of 40:60 (wt/wt %) and was coated from a dichloromethane solution containing 18-20 wt% total solids. Insolubility of the polybenzobisazoles in dichloromethane was essential to preparing well defined bilayer devices by this procedure. Single-layer thin films of the polymers on fused silica substrates for optical absorption spectra were prepared following the same procedure described above. The film thicknesses were measured by using a Tencor Northern Alpha Step profilometer. Optical absorption spectra of the single-layer and bilayer films were obtained with a Perkin Elmer Model Lambda 9 UV-Vis-near IR spectrophotometer in the wavelength range 190-3200 nm.

Xerographic Photoinduced Discharge Measurements

A schematic of the bilayer device and the experimental set up is shown in Figure 1. There are a number of advantages of the xerographic photoinduced discharge method for understanding photogeneration mechanism over conventional bulk photoconductivity measurements ($\sigma = ne\mu$).³³ The often difficult to realize ohmic contacts in bulk photoconductivity measurements is neither needed nor desirable in the photodischarge method. Also, one of the surfaces does not have to be electroded, thus allowing the device to be charged to a very high potential without breaking down. At low light intensities, and in the absence of deep trapping, this approach provides direct measurement of the quantum efficiency for photogeneration.³³

The photoinduced discharge experiments were performed by mounting each 5x5 cm^2 bilayer device in a xerographic cycling chamber designed so that either a corona

charger or a Monroe Electronics Model 114S-4 electrostatic voltmeter detector could be positioned in front of the sample. The device was charged to a desired surface potential (negative potential) with a corona charger supplied by a Universal Voltronics high-voltage source. An electrostatic voltage detector was placed in front of the device which was exposed to illumination from a xenon lamp passing through a Bausch and Lomb monochromator. The intensity of the exposing radiation, typically $0.3\text{--}5\text{ ergs/cm}^2\text{sec}$, was measured with an Optronics Laboratories Model 730A radiometer. The resulting photodischarge data was acquired with Keithley and analyzed with a computer program.

The quantum efficiency ϕ for photogeneration of charge carriers was determined from the initial rate of discharge of the device.³⁴ On the surface of the film, the amount of surface charge Q per unit area A is given by

$$\frac{Q}{A} = \frac{CV}{A} \quad (1)$$

where V is the surface potential and C is the film capacitance. Since ϕ is the number of surface charges lost per absorbed photon,

$$\phi = \frac{d(Q/eA)}{dt} \cdot \frac{1}{I} \quad (2)$$

where e is the electronic charge, I the photon intensity, and t is time. Taking C to be the geometric capacitance ($C = \epsilon\epsilon_0 A/l$) then ϕ becomes

$$\phi = \frac{\epsilon\epsilon_0}{el} \left[\frac{dV}{dt} \right]_{t=0} \quad (3)$$

where ϵ is the dielectric constant, ϵ_0 is the permittivity of free space, and l is the film thickness. All of the terms in Equation (3) are constant except dV/dt , the initial photoinduced discharge slope, which was determined by a least square analysis. The field-dependent quantum efficiency $\phi(E)$ was obtained by measuring the initial photodischarge at

different surface potentials. The field, E , across the device was taken to be V/l , where V is the surface potential and l is the total film thickness. This assumption ($E = V/l$) is true provided that the experiment is carried out under capacitive charging. As we will show later from the dark decay characteristics, the bilayer devices are indeed blocking, indicating that this assumption is valid. We used a Uniblitz Model 225L electronic shutter in combination with a Uniblitz Model 310B shutter timer control to expose the charged film for a fixed time of 1.2 s. The efficiency was based on the number of photons absorbed by the CGL layer. All measurements were made at ambient conditions.

Transient Absorption Spectroscopy

Picosecond transient absorption spectroscopy on a thin film of a single-layer PBZT and bilayer PBZT/TTA was carried out at room temperature as follows. The output from the third harmonic of a continuum PY61C picosecond laser was used to generate the pump beam and a residual 1064 nm beam was directed through an optical delay line and focused onto a 10 cm cell containing D₂O/phosphoric acid/deionized water (1:0.5:0.5 ratio by volume) to generate white light (400-950 nm). The beam was split 50 : 50; one part was used as the probe beam and the other used as a reference. The probe beam was focused onto the sample holder in such a way that it intersects the pump beam in the middle of the sample. The transmitted beams were focused onto a bifurcated fiber optic cable connected to a residual diode array optical multichannel analyzer detector (Princeton Instruments). The transient absorption data were obtained by collecting data in four runs, each run averaging about 100 shots. In the first run, both pump and probe beams were turned on while the excited state spectrum was collected. A ground state spectrum was then obtained by turning off the pump beam. The third run allowed the subtraction of any contribution from fluorescence of the sample by collecting the spectrum with the pump beam only. In the fourth run, both the pump and probe beams were turned off, and the background spectrum was obtained. The final transient absorption spectrum (difference spectrum) was obtained

by the usual Beer-Lambert law for the excited state and the ground state, correcting for luminescence and background absorption.

Photoluminescence Measurements

Steady state photoluminescence studies were done by using a Spex Fluorolog-2 Spectrofluorometer equipped with Spex DM3000f Spectroscopy computer. Fluorescence measurements were made on 15-40 nm single-layer polymer thin films and bilayers consisting of 15-40 nm thin films and a 200 nm TTA/PC overcoat. The polymer thin films were positioned such that the emission was detected at 22.5° from the incident radiation beam. The relative photoluminescence quantum efficiencies at different excitation wavelengths were obtained by comparing the integration of the emission spectra (total light emitted) with that at the λ_{max} , in the same optical configuration. Variation in the intensity of the exciting source with wavelength was accounted for by taking the spectra in the ratio mode (s/r); that is, by dividing the signal with that of rhodamine B which is used as the internal standard. Time-resolved photoluminescence decay measurements were performed by using time-correlated single photon counting (SPC) technique. The excitation system consisted of a cavity dumped dye laser (Coherent Model 703D) circulating rhodamine 6G, synchronously pumped by a mode-locked frequency doubled Nd:YAG laser (Quantronics Model 416). The dye laser pulses were typically of 10 ps duration at a repetition rate of 38 MHz and the samples were excited at 380 nm.

RESULTS AND DISCUSSION

Optical Absorption Spectra

The optical absorption spectra of single-layer thin films of the polymers and TTA as well as the bilayer polymer/TTA thin films were obtained in preparation for the photogeneration, photoluminescence, and transient absorption studies. The optical absorption spectrum of a thin sample of PBZT/TTA bilayer on a fused silica substrate is

shown in Figure 2 along with those of PBZT and TTA. The optical absorption spectrum of the PBZT/TTA bilayer is essentially a superposition of the two component absorption spectra. PBZT has absorption maxima (λ_{\max}) at 468, 438, and 256 nm whereas TTA dispersed in the matrix of polycarbonate has λ_{\max} at 300 nm. There are no new features or absorption bands in the spectrum of the PBZT/TTA bilayer that may indicate strong interactions between PBZT and TTA in the ground state. The optical absorption spectrum of the BBL/TTA bilayer on fused silica substrate, shown in Figure 3, also indicates a superposition of the component spectra. In all cases of the five conjugated polymer/TTA bilayers investigated, the absorption spectrum of each bilayer consisted of the component absorptions. The optical absorption maxima (λ_{\max}) of all the polybenzobisazole/TTA bilayers are summarized in Table 1 along with the optical properties of single-layer thin films of the polymers. The electronic spectra results indicate that bilayer assemblies of these polymers (A) which have weak electron accepting properties due to the benzobisazole ring and TTA which is a strong donor molecule (D) do not exhibit any significant ground state interaction. The TTA radical cation ($D^{+\cdot}$) which absorbs strongly at about 680 nm could not be detected in the absorption spectra of the bilayers. The absence of any significant ground-state interactions in the D/A bilayer assemblies makes the polybenzobisazole/TTA system a good one for probing photoinduced processes and charge photogeneration. Also in Table 1, we see that the energy of the onset of the lowest energy $\pi-\pi^*$ transition of the polybenzobisazoles varies between 1.78-2.76 eV, indicating a wide range of electronic structure variation with molecular structure. This should allow one to investigate the effect of structure on charge photogeneration in the conjugated polymers.

Photoinduced Discharge Curves

The bilayer device shown in Figure 1, is essentially a parallel-plate capacitor with the top electrode removed. When the top surface is charged in the dark by a corona, the bilayer must be blocking so that charge of the opposite polarity flows from the system

ground to the bottom plate (nickel coated PET), thus establishing an electric field within the bilayer. Exposure of the surface charged bilayer device to light allows one to determine many photophysical parameters of the bilayer. Figure 4 shows the photoinduced discharge curve of freshly prepared bilayer assemblies of four polymers with TTA that were charged to different initial surface potentials. The flat portion of the curves represents the dark decay and corresponds to decay rates of 0.2-0.8 V/s for the four bilayers. When a PBZT/TTA bilayer device, for example, was illuminated at 470 nm near the absorption maximum of PBZT, charges are photogenerated and transported through the TTA/PC layer (CTL) to neutralize the surface charge. Only holes are mobile in the CTL and the hole mobility in the TTA/PC layer is on the order of 10^{-5} cm²/Vs at an applied field of 10^5 V/cm.³⁵ The photon energy required to discharge the surface potential to half its original value, known as the photosensitivity ($E_{1/2}$), is 12 ergs/cm² for the PBZT/TTA bilayer device based on absorbed photons. This photosensitivity is comparable to those reported for some N,N'-disubstituted perylene dyes.³⁶ The residual potential (V_r) of the PBZT/TTA bilayer at an exposure of 80 ergs/cm² in Figure 4 is ~ -20 V, which is 4.3% of the initial surface potential of -460 V.

The photoinduced discharge curves for other polymer/TTA bilayer devices shown in Figure 4 indicate that PBZT/TTA is the most photosensitive. A summary of the photosensitivity and dark decay characteristics is given in Table 2 for freshly prepared polymer/TTA bilayers, indicating $E_{1/2}$ of 12-27 ergs/cm². The PBO/TTA bilayer system is the least sensitive, requiring 27 ergs/cm² to discharge the surface potential to half its original value. The variation of the photosensitivity ($E_{1/2}$) of the different polymer/TTA bilayer assemblies may be due to a number of factors which include the polymer molecular structure, the nature of the bilayer interface, and trapping of photogenerated carriers to varying degrees in the bilayers.

The dark decay characteristics show that these bilayers are blocking. This implies

that the assumption of capacitive charging is valid for these bilayers. Also, there is negligible built-in potentials at the polymer/TTA interfaces when the bilayer devices were freshly prepared, suggesting that there are no trapped carriers due to energy mismatch at the bilayer interface prior to illumination. Although repeated charging and photodischarge cycling subsequently leads to an increase in the dark decay, typically to ~ 4 V/s, the dark decay characteristics even after repeated charging are still much better than the vast number of photoreceptor systems, published in a recent review^{25a}, in which the dark decay varied from -2.5 to -115 V/s. At sufficient exposures, all the devices decayed to zero surface potential, indicating that there is minimal trapping of charge carriers in the bilayer devices. The high exposure needed to reduce the surface potential to zero reflects the strong field dependence of the mobility at low fields.

The photoinduced discharge curves were found to be well described by an exponential function commonly used in the evaluation of bilayer photoconductive materials employed in high-speed printing³⁷:

$$V_l = V_r + (V_o - V_r) \exp\left(\frac{-E}{E_a}\right) \quad (4)$$

where V_l is the light voltage (i.e. the surface potential when the device is exposed to light), V_o is the initial surface potential in the dark, V_r is the residual potential at high exposures (E), and E_a is a sensitivity (exposure) constant which is another measure of the photosensitivity of the device. A typical empirical fit (Equation 4) of the photodischarge curves exemplified with the BBL/TTA bilayer is shown in Figures 5. The sensitivity E_a obtained from the fit of the photoinduced discharge curves of the polymer/TTA bilayers is given in Table 2. The trend of E_a is similar to that observed for $E_{1/2}$ in the bilayers. The value of $E_{1/2}$ describes the special case where V_l is $V_o/2$, whereas E_a represents the complete photodischarge to an asymptotic V_r .

Charge Photogeneration Quantum Efficiency

The quantum efficiency for photogeneration of charge carriers in bilayer layer devices as calculated from equation (3) carries an implicit assumption: that all the photogenerated charge carriers injected into the charge transport layer reach the charged free surface. If trapping in the CGL, CTL or at the CGL/CTL interface are significant factors, the ϕ calculated by equation (3) is only a lower limit. Also, it is assumed in equation (3) that ϕ is independent of light intensity. This assumption can be checked by rearranging equation (3) in the form:

$$\left[\frac{dV}{dt} \right]_{t=0} = \left(\frac{\phi e l}{\epsilon \epsilon_0} \right) \cdot I \quad (5)$$

Equation (5) implies that at constant field, the initial rate of photodischarge is proportional to the incident light intensity. Figure 6 shows a plot of the initial rate of photoinduced discharge of a PBZT/TTA bilayer versus the light intensity, at an electric field of 2.4×10^5 V/cm. A linear relationship is obtained, confirming the validity of the assumption. The limit of the linear dependence of $[dV/dt]_{t=0}$ on intensity at constant field was further investigated with a sample of BBL/TTA excited at 568 nm. This wavelength was chosen because the intensity of the Xenon lamp used in these measurements is higher at 568 nm, the λ_{max} of BBL, than at 470 nm. The inset of Figure 6 shows a plot of the initial rate of photodischarge at an electric field of 2.48×10^5 V/cm versus absorbed photon intensity. At higher intensities (>15 ergs/cm²), deviation from the linear relationship is observed. The quantum efficiency for photogeneration in all the bilayer devices were measured at photon intensities between 0.3-5 ergs/cm². This implies that the measured photogeneration quantum efficiencies were under emission limited conditions, i.e. the number of charges moving through the film at any time is much less than the surface charge at that time.

Figure 7 shows the field-dependent quantum efficiency $\phi(E)$ for photogeneration in PBZT/TTA and PBBZT/TTA bilayers excited at 470 and 430 nm, respectively. $\phi(E)$

appears to exhibit essentially two regimes. At low fields ($< 2 \times 10^4$ V/cm) photogeneration efficiency is relatively independent of field whereas a strong field dependence of $\phi(E)$ is observed at higher fields. In the case of a PBZT/TTA bilayer, $\phi(E)$ at low field is 10^{-2} , whereas at 10^6 V/cm, $\phi(E)$ increases dramatically to 0.32. The $\phi(E)$ values of PBBZT/TTA ranges from $\sim 10^{-3}$ at low fields ($< 2 \times 10^4$ V/cm) to 0.14 at 7×10^5 V/cm, whereas in the case of PBO/TTA, $\phi(E)$ was 7×10^{-3} at low fields (2×10^4 V/cm) and increased to 0.12 at 3×10^5 V/cm. Figure 8 shows the field dependence of the quantum efficiency for photogeneration in a PBTPV/TTA bilayer. The shape of $\phi(E)$ is similar to that observed in the PBZT/TTA bilayer. At low fields, ϕ has a weak dependence on field and approaches 10^{-2} at an electric field of 7×10^3 V/cm. A much stronger field dependence is observed at higher fields where ϕ increases to ~ 0.14 at 3×10^5 V/cm.

An illustration of the effect of the hole transporting triarylamine layer on $\phi(E)$ is shown in Figure 9 for BBL/TTA and BBL/TPD bilayers. The $\phi(E)$ results for BBL/TPD bilayer were previously reported¹⁹ and are shown in the figure for comparison with the present results for BBL/TTA. Although the field dependence of the quantum yield in both cases shows a similar trend as the other bilayers discussed above, the photocarrier yield in the BBL/TTA bilayer is larger by up to an order of magnitude at high fields ($> \sim 10^5$ V/cm). The reason for the large difference in $\phi(E)$ for BBL/TTA and BBL/TPD bilayers is not obvious. The oxidation potential of TPD ($E^\circ_{ox} = -0.8$ V versus SCE)^{38,39} is very close to that of TTA (0.74 V versus SCE)⁴⁰ and the hole mobilities in the TTA/PC and TPD/PC layers are likewise similar.^{35,41} Further investigation of the role of the donor hole transporting layer on $\phi(E)$ was made on PBZT/poly(N-vinyl carbazole) (PVK) bilayer and in single layer thin films of the conjugated polymers. In the former case, the measured quantum yield at 5×10^5 V/cm was 0.005 which is a factor of about 50 less than in PBZT/TTA bilayer. In the latter case of single layer thin films of the polymers the $\phi(E)$ was unmeasurably small. These results clearly show that the donor layer is essential to efficient

photocarrier production in the bilayers and furthermore that the quantum yield also depends on the nature of the donor layer.

Mechanism of Photogeneration

An understanding of the mechanism of charge photogeneration in these materials is needed to account for the observations on quantum yield dependencies on electric field, polymer structure, bilayer composition, and the donor hole transport layer. The strong field dependence of quantum efficiency for photogeneration in the bilayers and the functional form of the $\phi(E)$ data suggests the applicability of Onsager's theory of geminate ion-pair dissociation.^{24,26} In particular, the weak field dependence of $\phi(E)$ at low fields which indicates a finite photogeneration at zero field is reminiscent of Onsager's three-dimensional probability for an ion-pair to escape geminate recombination.^{24,26} In contrast, the one-dimensional version of Onsager's model was found to best describe charge photogeneration $\phi(E)$ data in PPV derivatives and polydiacetylenes.^{5,6} In both the polydiacetylenes and PPV derivatives the geminate ion-pair is an exciton localized on a single polymer chain. What remains to be clarified in this mechanistic picture of photogeneration in our materials are the following questions: (i) what are the geminate ion-pairs?; and (ii) where is the dissociation of ion-pairs occurring in the bilayers, is it in the bulk of the polymer layer or at the bilayer interface? The latter question can also be cast in terms of *intrinsic* (bulk) versus *extrinsic* (interface) dissociation of the geminate ion-pairs. We will first address the issue of the nature of the photogenerated ion-pairs.

The nature of photoexcitations in the π -conjugated polymers was investigated in part by picosecond transient absorption spectroscopy. This is essentially a pump and probe experiment in which the polymer is photoexcited and the excited state species probed with white light continuum (400-950 nm). Figure 10 shows the transient absorption spectra of a thin film of pristine PBZT excited at 355 nm and probed at 125 and 200 ps delays. Each transient absorption spectrum represents the difference between the excited state and the

ground state absorption spectra, after correcting for luminescence and background absorption. The photoinduced bleaching (negative absorbance) seen in Figure 10 implies that the absorption features are only present in the ground state spectra. At early times (≤ 125 ps), there is a positive transient absorption near the $\pi-\pi^*$ absorption edge (500 nm) of PBZT, but it disappears very rapidly. At 200 ps and beyond, there was no excited state species that absorb between 400-950 nm at room temperature. No transient absorption characteristic of the creation of *polarons* or *bipolarons* was detected within the resolution of our instrument (~ 75 ps). The transient absorption near 500 nm which was detected at 125 ps may be due to *excitons*. Excitons have also been observed as the primary photogenerated species at the $\pi-\pi^*$ absorption edge of BBL by femtosecond transient absorption spectroscopy.⁴² The better temporal resolution (~ 100 fs) in this experiment allowed us to probe the dynamics of the photogenerated species and their assignment as *excitons*. These results suggest that the primary photoexcitations in the polybenzobisazoles are excitonic in nature, similar to the polydiacetylenes^{6,43,44} and poly(2-phenyl-1,4-phenylenevinylene).⁵

Our recent studies²³ of the conjugated polybenzobisazoles in different forms (fluid solutions, solid solutions, and thin films) by steady-state and time-resolved photoluminescence spectroscopy showed that the photogenerated excitons rapidly (< 200 ps) formed intermolecular excimers: $^1A^* + ^1A = ^1(AA)^*$. Such interchain photoinduced processes can be expected to be important in steady-state photogeneration such as in the xerographic photoinduced discharge experiments.

The case that charge photogeneration in the bilayers, i.e. dissociation of ion-pairs, occurs at the interface will be made on the basis of a number of experimental observations, including: wavelength dependence of photogeneration quantum yield; and exciplex formation at the interface. The excitation wavelength dependence of the steady state photoluminescence of PBZT thin film is shown in Figure 11. We see that irrespective of

the excitation wavelength between 400-470 nm, the emission λ_{max} is at 564 nm, suggesting that emission is from the same singlet manifold. The quantum efficiency for producing this singlet emitting state based on absorbed photons is independent of wavelength as shown in Figure 12. This implies that if photogeneration involves electric field dissociation of singlet excitons (binding energy $\sim 0.4\text{-}0.5\text{ eV}$)²³ in the bulk following photoexcitation, at constant field, there should be equal probability for dissociation irrespective of the excitation wavelength. This means that the quantum yield for intrinsic photogeneration in the bilayers should be independent of wavelength. However, as we shall show shortly, the quantum efficiency for photogeneration depends on wavelength.

According to a one-dimensional model^{46,47} for the creation of excitons in the CGL and subsequent diffusion to the bilayer interface for thick samples, where the exciton diffusion length (L) and absorption depth ($1/\alpha$) are much less than the thickness (d) of the CGL, all of the incident photons are absorbed ($I = I_0$), and $e^{d/L} \gg e^{-d/L}$, ϕ is related to α :

$$\phi^{-1} = \left\{ \frac{1}{bL} \right\} \cdot \alpha^{-1} + \frac{1}{b} \quad (6)$$

This implies that a plot of $1/\phi$ versus $1/\alpha$ should yield a straight line with an intercept-to-slope ratio of L , the exciton diffusion length. In equation 6, b is a constant. Figure 13 shows that this linear relationship between $1/\phi$ and $1/\alpha$ holds for a $\sim 1\text{ }\mu\text{m}$ thin film of PBZT used as the charge generation layer. The best fit of the data gives an intercept-to-slope ratio of $1.84 \times 10^{-6}\text{ cm}$. This means that the exciton diffusion length in PBZT is 184 Å. This is comparable to the estimated diffusion length of excitons in poly(*p*-phenylene vinylene) (PPV)^{18b} which is between 100-200 Å. The typical exciton diffusion length for a good quality anthracene crystal⁴⁷ is between 400-600 Å whereas a poor quality anthracene crystal has a diffusion length of $\sim 200\text{ Å}$.⁴⁷ For a very thin film of the CGL such that the incident photon is absorbed throughout the sample and $L \ll 1/\alpha$ we have :

$$\phi = bL\alpha \quad (7)$$

In this case, the quantum efficiency is directly proportional to the absorption coefficient. Figure 14 shows that this predicted behavior is exhibited by a ~15 nm thin film of PBZT. The quantum efficiency at a field of 2.5×10^5 V/cm tracks the optical absorption spectrum fairly well between the λ_{max} and the higher energy region. These results suggest that the dominant charge photogeneration mechanism in the polymer/triarylamine bilayers occurs at the interface.

We recently showed by a combination of transient (ps) absorption, steady-state photoluminescence, and time-resolved (ps) photoluminescence (PL) decay dynamics studies on the same polymer/TTA bilayer assemblies that *exciplexes* are formed at the interface.^{18,23} Although no ground-state charge transfer complex is formed between the weak electron accepting conjugated polybenzobisazole (A) and the donor molecule TTA (D), an excited-state charge transfer complex is formed on photoexcitation of the polymer in the bilayer: $^1A^* + ^1D = ^1(A \cdots D^+)^*$. Figure 15 shows a comparison of the transient absorption spectrum of a PBZT/TTA bilayer excited at 355 nm and a solution optical absorption spectrum of a known TTA^+ . Clearly, the peak of the PBZT^{*}/TTA transient absorption spectrum at ~680 nm is due to the TTA^+ radical cation, formed by photoinduced electron transfer from TTA to the excited PBZT. The dynamics of the excited state species was probed by taking transient absorption spectra at different delays from 125 ps to 7 ns. Figure 16 shows a plot of the peak absorbance versus time. The dynamics shows that the TTA^+ is formed in ~150 ps, reaching a maximum intensity at 200 ps. The intensity decays rapidly within the first 1 ns, but persists up to 7 ns, at room temperature. The results of the transient absorption spectroscopy are consistent with the proposed mechanism that photogeneration in the polybenzobisazole/TTA bilayers occurs by ion-pair dissociation at the bilayer interface. Furthermore, the ion-pairs are the radical ion pairs ($A \cdots D^+$) produced by exciplex formation. The *intermolecular nature* of the ion-pairs is consistent with the similarity of the $\phi(E)$ data to the 3-D Onsager model²⁴ for ion-pair

dissociation.

Steady-state and time-resolved PL decay dynamics of the polymer^{*}/TTA bilayers confirmed the formation of *exciplexes* with distinct luminescent properties compared to the component single layer materials. A summary of the steady-state PL spectra of the pristine polymers and the corresponding polymer^{*}/TTA bilayer assemblies is given Table 3. The exciplex emission maxima are blue shifted by 26-80 nm relative to the pristine polymer thin film emission spectra which are due to intermolecular excimers.²³ That the exciplex emission is from the interface was further evidenced by the variation of the relative PL quantum efficiency of the polymer^{*}/TTA bilayers with the absorption depth in the photoexcited polymer. Figure 17 shows the PL decay dynamics of a typical polymer^{*}/TTA bilayer (PBO^{*}/TTA) along with that of the pristine polymer. It is observed that the PL decay of the bilayer does not follow a single exponential decay route, similar to the pristine polymer film. However, the lifetime of the exciplex emission is significantly longer than that of the polymer thin film. The initial rapid decay observed in the exciplex emission is due to the time required to form the exciplex, ~0.2 ns, as observed from the transient absorption experiments. Most of the initial decay comes from the pristine polymer but once the exciplex is formed, the lifetime increases rapidly to 4.6 ns in the case of PBO^{*}/TTA. A film of TTA/polycarbonate excited at 300 nm has a lifetime of 2.9 ns, while a film of PBO excited at 380 nm has two exponential lifetimes of 0.05 and 0.66 ns.

Given our proposed model of charge photogeneration in the bilayer assemblies, i.e. photoinduced electron transfer at the bilayer interface and formation of intermolecular exciplexes whose radical ion pairs are dissociated in electric field according to Onsager's three-dimensional probability for geminate recombination²⁴, the observed quantum yields $\phi(E)$ in the different bilayers can be rationalized qualitatively. The field dependent quantum yield $\phi(E)$ can be understood as the product of the initial ion-pair quantum yield ϕ_0 and the field dependent Onsager's probability for geminate ion-pair recombination $f(E)$ ²⁶:

$$\phi(E) = \phi_o f(E) \quad (8)$$

If k_{et} is the rate constant for electron transfer and k_{pl} is the sum of the rate constants for all other decay processes of the photoexcited conjugated polymer or bilayer, the initial ion-pair quantum yield is given by:

$$\phi_o = \frac{k_{et}}{k_{et} + k_{pl}} \quad (9)$$

The observed similarity of the field dependence of the quantum yield data for the different bilayers arises from: (i) similarity of $f(E)$ since the same Onsager process is involved and (ii) similarity of the ion-pair state intermediate in free carrier generation. On the other hand, the observed differences in the magnitude of $\phi(E)$ in the different bilayers can be accounted for by variation in the initial ion-pair quantum yield ϕ_o and hence all factors that affect exciplex formation/electron transfer and extent of charge transfer. Prominent among these factors are the molecular geometries of the conjugated polymers (A) and triarylamine donors (D), the supramolecular structure of triarylamine/conjugated polymer exciplexes, and the energetics of the electron transfer/exciple formation.

A consideration of these factors in the case of PBZT/TTA and PBBZT/TTA bilayers rules out energetics of electron transfer as the source of the difference in the magnitude of $\phi(E)$ (see Figure 7). This is because an estimate of the free energies ($E_D^{ox} - E_A^{ox}$) of the electron transfer in the two bilayers shows that they are similar. It appears that the main reason for the difference in $\phi(E)$ data is the structure of the polymers involved and of their exciplexes with TTA. The order of magnitude difference in $\phi(E)$ between BBL/TTA and BBL/TPD (Figure 9) is similarly attributable to geometric factors since E_D^{ox} is similar in the two donors (0.74 V versus 0.8 V, relative to SCE).^{38,40} The rather low quantum yield observed in the PBZT/PVK bilayer, about a factor of 50 less than in the PBZT/TTA bilayer, is likely due to the poor efficiency for exciplex formation/electron transfer. Although the free energy ($\Delta G^o \sim E_D^{ox} - E_A^{ox} \leq -0.3$ eV) appears favorable, the covalent

binding of the carbazole donor molecules to a polymer chain imposes severe barriers to favorable interaction with the rodlike PBZT molecules.

Finally, we point out the reasons for the large enhancement of $\phi(E)$ in the bilayers compared to the extremely small quantum yields (not measurable in the present xerographic photoinduced discharge experiment) for photocarrier generation in single layers of the pristine conjugated polymers. In the absence of a donor molecule layer as discussed previously, photoexcitations of thin films of the conjugated polymers produces *excitons* which readily form *excimers*. The initial ion-pair quantum yield ϕ_0 in this case would depend on the relative contributions of exciton and charge transfer configurations to the excimer structure. The greater charge transfer character of *exciplexes* compared to excimers means that both ϕ_0 and $f(E)$ should be significantly larger in the exciplexes. Thus photoinduced charge transfer and exciplex formation enhance $\phi(E)$ because these processes lead to efficient production of radical ion-pairs which are highly polar species that can readily dissociated by electric field. Our results on enhanced charge photogeneration in triarylamine/conjugated polybenzobisazole exciplexes when taken together with prior reports on enhanced photoconductivity in C_{60} /PPV¹⁵ and C_{60} /polythiophene¹⁶ suggest a more general phenomenon: exciplexes of conjugated polymers exhibit enhanced charge photogeneration and photoconductivity.

CONCLUSIONS

Photogeneration of charge carriers in π -conjugated rigid-rod polybenzobisazoles in bilayer assemblies with triarylamine doped polycarbonate has been investigated by the xerographic photoinduced discharge technique along with picosecond photoinduced absorption and luminescence spectroscopies. The measured electric field dependent quantum yield $\phi(E)$ of photocarrier generation was large, suggesting that the materials are

good photoconductors that might find applications in optoelectronic devices. Our proposed model of the photocarrier generation process in the bilayers is that photoinduced electron transfer and exciplex formation occur at the bilayer interface, resulting in intermolecular exciplexes as the geminate ion-pairs which are dissociated in electric field according to Onsager's three-dimensional probability. The similarity and differences among the quantum yield data for the various conjugated polymers and bilayers are rationalized satisfactorily by this model.

Our results showing large enhancement of charge photogeneration in triarylamine/conjugated polybenzobisazoles along with prior reports of enhanced photoconductivity in C₆₀/poly(phenylene vinylenes)¹⁵ and C₆₀/polythiophenes¹⁶ constitute important examples of a general phenomenon: conjugated polymer exciplexes exhibit enhanced charge photogeneration and photoconductivity relative to the pristine conjugated polymers.

ACKNOWLEDGEMENTS

This research was supported by the Office of Naval Research, the National Science Foundation Center for Photoinduced Charge Transfer (Grant CHE-9120001) and the National Science Foundation (Grant CTS-9311741). The financial support of a Link Foundation Fellowship to J. A. O. is also appreciated. We thank T. Buranda for technical assistance in the transient absorption experiments.

REFERENCES

1. (a) Etemad, S.; Mitani, T.; Ozaki, M.; Chung, T. C.; Heeger, A. J.; MacDiarmid, A. G. *Solid State Commun.* **1981**, *40*, 75-79. (b) Lauchlan, L.; Etemad, S.; Chung, T. C.; Heeger, A. J.; MacDiarmid, A. G. *Phys. Rev. B* **1981**, *24*, 3701-3711.
2. Bleier, H.; Roth, S.; Shen, Y. Q.; Schafer-Siebert, D.; Leising, G. *Phys. Rev. B* **1988**, *38*, 6031-6040.
3. Moses, D.; Sinclair, M.; Heeger, A. J. *Phys. Rev. Lett.* **1987**, *25*, 2710-2713.
4. (a) Tokito, S.; Tsutsui, T.; Tanaka, R.; Saito, S. *Jap. J. Appl. Phys.* **1986**, *25*, L680-L681. (b) Bleier, H.; Shen Y. Q.; Bradley, D. D. C.; Lindenberger, H.; Roth, S. *Synth. Metals* **1989**, *29*, E73-E78.
5. Gailberger, M.; Bassler, H. *Phys. Rev. B* **1991**, *44*, 8643-8651.
6. (a) Bassler, H. in *Polydiacetylene*, Bloor, D. and Chance, R. R., Eds., Martinus Nijhoff: Dordrecht, Netherlands, 1985; p.135. (b) Donovan, K. J.; Freeman, P. D.; Wilson, E. G. *Mol. Cryst. Liq. Cryst.* **1985**, *118*, 395-401.
7. Yu, G.; Phillips, S. D.; Tomozawa, H.; Heeger, A. J. *Phys. Rev. B* **1990**, *42*, 3004-3010.
8. Abkowitz, M. A.; Stolka, M.; Antoniadis, H.; Agrawal, A. K.; Jenekhe, S. A. *Solid State Commun.* **1992**, *83*, 937-941.
9. Heeger, A. J.; Kivelson, S.; Scheiffer, R. J.; Su, W. P. *Rev. Mod. Phys.* **1988**, *60*, 781-850.
10. (a) Hsu, J. W. P.; Yan, M.; Jedju, T. M.; Rothberg, L. J.; Hsieh, B. R. *Phys. Rev. B* **1994**, *49*, 712-719. (b) Yan, M.; Rothberg, L. J.; Papadimitrakopoulos, F.; Galvin, M. E.; Miller, T. M. *Phys. Rev. Lett.* **1994**, *72*, 1104-1106.
11. Rauscher, U.; Bassler, H.; Bradley, D. D. C.; Hennecke, M. *Phys. Rev. B* **1990**, *42*, 9830-9836.
12. (a) McCall, R. P.; Ginder, J. M.; Leng, J. M.; Ye, H. J.; Manohar, S. K.;

- Masters, J. G.; Asturias, G. E.; MacDiarmid, A. G.; Epstein, A. J. *Phys. Rev. B* **1990**, *41*, 5202-5213.
13. Brassett, A. J.; Colaneri, N. F.; Bradley, D. D. C.; Lawrence, R. A.; Friend, R. H.; Murata, M.; Tokito, S.; Tsutsui, T.; Saito, S. *Phys. Rev. B* **1990**, *41*, 10586-10594.
 14. Woo, H. S.; Graham, S. C.; Halliday, D. A.; Bradley, D. C. C. *Phys. Rev. B* **1992**, *46*, 7379-7389.
 15. (a) Sariciftci, N. S.; Smilowitz, L.; Heeger, A. J.; Wudl, F. *Science*, **1992**, *258*, 1474-1476. (b) Lee, C. H.; Yu, G.; Moses, D.; Pakbaz, K.; Zhang, C.; Sariciftci, N. S.; Heeger, A. J.; Wudl, F. *Phys. Rev. B* **1993**, *48*, 15425-15433.
 16. Yoshino, K.; Yin, X. H.; Morina, S.; Kawai, T.; Zakhidov, A. A. *Solid State Commun.* **1993**, *85*, 85-88. (b) Morita, S.; Zakhidov, A. A.; Yoshino, K. *Solid State Commun.* **1992**, *82*, 249-252.
 17. Osaheni, J. A.; Jenekhe, S. A.; Perlstein, J. *Appl. Phys. Lett.* **1994**, *64*, 3112-3114.
 18. Osaheni, J. A.; Jenekhe, S. A. *Macromolecules* **1994**, *27*, 739-741.
 19. Antoniadis, H.; Abkowitz, M. A.; Osaheni, J. A.; Jenekhe, S. A.; Stolka, M. *Synth. Metals* **1993**, *60*, 149-157.
 20. (a) Antoniadis, H.; Abkowitz, M. A.; Hsieh, B. R.; Stolka, M. *Appl. Phys. Lett.* **1993**, *62*, 3167-3169. (b) Antoniadis, H.; Abkowitz, M. A.; Hsieh, B. R.; Jenekhe, S. A.; Stolka, M. *Mol. Cryst. Liq. Cryst.* **1994**, in press.
 21. (a) Burroughes, J. H.; Bradley, D. D. C.; Brown, A. R.; Marks, R. N.; Mackay, K.; Friend, R. H.; Burn, P. L.; Holmes, A. B. *Nature* **1990**, *347*, 539-541. (b) Gustafsson, G.; Cao, Y.; Treacy, G. M.; Klavetter, F.; Colaneri, N.; Heeger, A. J. *Nature*, **1992**, *357*, 477-479.

22. Antoniadis, H.; Hsieh, B. R.; Abkowitz, M. A.; Stolka, M.; Jenekhe, S. A. *Synth. Metals* **1994**, *62*, 265-271.
23. Jenekhe, S. A.; Osaheni, J. A. *Science* **1994**, in press.
24. (a) Onsager, L. *J. Chem. Phys.* **1934**, *2* 599-615 (b) Onsager, L. *Phys. Rev.* **1938**, *54*, 554-557.
25. (a) Law, K-Y. *Chem. Rev.* **1993**, *93*, 449-486. (b) Borsenberger, P. M.; Weiss, D. S. in *Handbook of Imaging Materials*, Diamond, A. S. Ed.; Marcel Dekker; New York: 1991, p.379-446.
26. Pai, D. M.; Springett, B. E. *Rev. Mod. Phys.* **1993**, *65*, 163-211.
27. (a) Jenekhe, S. A.; Johnson, P. O.; Agrawal, A. K. *Macromolecules* **1989**, *22*, 3216-3222. (b) Jenekhe, S. A.; Johnson, P. O. *Macromolecules* **1990**, *23*, 4419-4429.
28. Osaheni, J. A.; Jenekhe, S. A. *Chem. Mater.* **1992**, *4*, 1282-1290.
29. (a) Osaheni, J. A.; Jenekhe, S. A. *Macromolecules* **1993**, *26*, 4726-4728.
(b) Osaheni, J. A.; Jenekhe, S. A. Manuscript in preparation.
30. Jenekhe, S. A.; Osaheni, J. A.; Vanherzeele, H.; Meth, J. *Chem. Mater.* **1992**, *4*, 683-687.
31. (a) Meth, J. S.; Vanherzeele, H.; Jenekhe, S. A.; Roberts, M. F.; Agrawal, A. K.; Yang, C. J. *SPIE* **1991**, *1560*, 13-24. (b) Vanherzeele, H.; Meth, J. S.; Jenekhe, S. A.; Roberts, M. F. *J. Opt. Soc. Am. B* **1992**, *9*, 524-532.
32. Torruellas, W. E.; Cha, M.; Stegeman, G. I.; Osaheni, J. A.; Jenekhe, S. A. *J. Opt. Soc. Am. B*, Submitted.
33. Mort, J.; Pfister, G. *Electronic Properties of Polymers*, Wiley: New York; 1982, Chapter 6.
34. Mort, J.; Chen, I. *Appl. Solid State Sci.* **1975**, *5*, 69-149.
35. Borsenberger, P. M. *J. Appl. Phys.* **1990**, *68*, 6263-6273.

36. Loutfy, R. O.; Hor. A. M.; Kazmaier, P.; Tan, M. J. *Imaging Sci.* **1989**, *33*, 151.
37. Williams, E. M. *The Physics and Technology of Xerographic Processes*, Wiley-Interscience; New York: 1984, p.16-37.
38. Yuh, H. J.; Abramsohn, O.; Stolka, M. *Phil. Mag. Lett.* **1987**, *55*, 277-282.
39. Loutfy, R. O.; Hor. A. M.; Kazmaier, P. M.; Burt, R. A.; Hamer, G. K. *Dyes and Pigments* **1991**, *15*, 139-156.
40. Gordon, M.; Ware, W. R., Eds. *The Exciplex*, Academic Press; New York: 1975.
41. Pai, D. M. in *Frontiers of Polymer Research*, Prasad, P. N. and Nigan, J. K. Eds., Plenum: New York, 1991, p.315-333.
42. (a) Weng, X.; Osaheni, J. A.; Jenekhe, S. A.; Fauchet, P. M. *Bull. Am. Phys. Soc.* **1994**, *39*, 337. (b) Manuscript in preparation.
43. Etemad, S.; Baker, G. L.; Orenstein, J.; Lee, K. M. *Mol. Cryst. Liq. Cryst.* **1985**, *118*, 389-393.
44. Robins, L.; Orenstein, J.; Superfine, R. *Phys. Rev. Lett.* **1986**, *56*, 1850-1853.
46. Simpson, O. *Proc. Royal. Soc. London. Ser. A* **1956**, *238*, 402-411.
47. Perlstein, J. H.; Borsenberger, P. M. in *Extended Linear Chain Compounds*, Miller, J. S. Ed., Plenum; New York: 1982, vol. 2, p.339-384.

Table 1. Summary of Optical Absorption Spectra of single-layer Polybenzobisazoles and their bilayers with TTA.

Material	Single-Layer			Polymer/TTA Bilayer λ_{\max} (nm)
	λ_{\max} (nm)	α (cm ⁻¹)	$\pi-\pi^*$ Energy gap (eV)	
PBZT	468 438 256	1.7x10 ⁵	2.48	468 438 300 256
PBBZT	415 246	1.01x10 ⁵	2.61	415 300 246
PBTPV	508 475 252	1.6x10 ⁵	2.1	508 475 300 252
PBO	427 401	2.4x10 ⁵	2.76	427 401 300
BBL	568 351 210	1.0x10 ⁵	1.78	568 351 300 210
TTA/PC (40:60)	300	3.57x10 ⁴	3.54	-

Table 2. Summary of Photosensitivity and Dark Decay of Polybenzobisazole/TTA Bilayer Devices

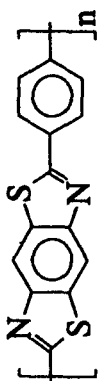
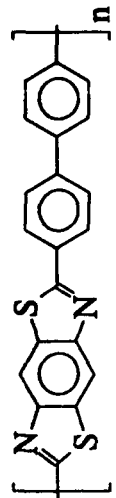
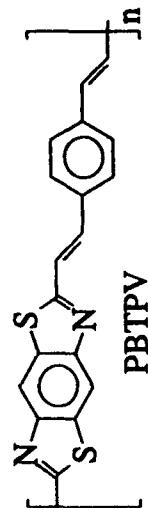
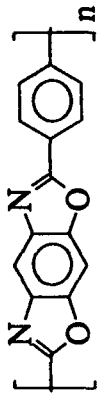
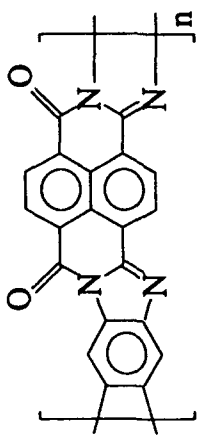
Polymers	Initial Surface Potential, V_0 (volts)	Dark Decay (volts/s)	Photosensitivity $E_{1/2}$ (ergs/cm ²)	E_a (ergs/cm ²)
 PBZT	-460	~0.4	12	16
 PBBZT	-550	~0.2	20	27
 PBTPV	-450	~0.4	16	23
 PBO	-520	~0.8	27	46
 BBL	-540	~0.2	18	24

Table 3. Photoluminescent properties of bilayer polybenzobisazoles/tris(*p*-toyl)amine exciplexes.

Polymers	Single Layer		Polymer/TTA Bilayer ^a
	Film Thickness (nm)	Emission λ_{max} (nm)	Exciplex Emission λ_{max} (nm)
PBZT	35	564	512
PBBZT	40	536	490
PBTPV	40	640	560
PBO	15	500	474

a. The TTA/Polycarbonate layer was 200 nm thick.

FIGURE CAPTIONS

Figure 1. Schematic of xerographic photoinduced discharge measurement on a bilayer device consisting of a π -conjugated polymer as the charge generation layer and tris(*p*-tolyl)amine as charge transporting layer.

Figure 2. Optical absorption spectra of thin films of: (1) PBZT; (2) PBZT/TTA bilayer; and (3) TTA dispersed in polycarbonate.

Figure 3. Optical absorption spectra of thin films of: (1) BBL; (2) BBL/TTA bilayer; and (3) TTA dispersed in polycarbonate.

Figure 4. Photoinduced discharge curves of polymer/TTA bilayer assemblies: (a) PBO/TTA, (b) PBBZT/TTA, (c) PBTPV/TTA, and (d) PBZT/TTA, charged to different initial surface potentials and excited at their respective absorption λ_{max} .

Figure 5. Photoinduced discharge curve of BBL/TTA bilayer device excited at 568 nm along with the exponential fit of the data (open circle: experimental data; solid line: fit of the data).

Figure 6. Initial Photoinduced discharge slope of PBZT/TTA bilayer versus photon intensity at an electric field of 2.4×10^5 V/cm. Initial Photoinduced discharge slope of BBL/TTA bilayer versus photon intensity at an electric field of 2.48×10^5 V/cm is shown in the inset.

Figure 7. Quantum efficiency, ϕ , versus electric field: (1) PBZT/TTA bilayer device at 470 nm; (2) PBBZT/TTA bilayer device at 430 nm.

Figure 8. Quantum efficiency of PBTPV/TTA bilayer device versus electric field at 475 nm.

Figure 9. Quantum efficiency versus electric field showing the effect of the hole

transporting layer. (1) BBL/TTA bilayer device; (2) BBL/TPD bilayer device.

Figure 10. Transient Absorption spectra of PBZT: (1) Pump-probe delay = 125 ps; (2) Pump-probe delay = 200 ps.

Figure 11. Photoluminescence spectra of PBZT thin film at various excitation wavelengths from 400 to 470 nm.

Figure 12. Optical absorption spectrum of thin film of PBZT (solid line) and the relative Photoluminescence yield at different excitation wavelengths (filled circle). The dash line is to guide the eye.

Figure 13. Plot of the reciprocal of quantum efficiency of photogeneration ($1/\phi$) at 2.5×10^5 V/cm versus absorption depth ($1/\alpha$) in a 1 μm PBZT charge generation layer.

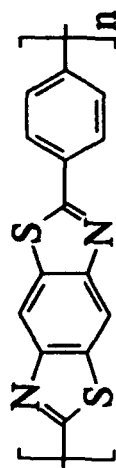
Figure 14. Optical absorption spectrum of a 15-nm PBZT film (solid line) and a plot of the quantum efficiency of photogeneration at 2.5×10^5 V/cm versus wavelength (filled circles).

Figure 15. Comparison of the transient absorption spectra of PBZT/TTA bilayer film with that of the solution optical absorption spectrum of TTA⁺: (1) PBZT/TTA bilayer; (2) TTA dissolved in CH_2Cl_2 with a few drops of methanesulfonic acid.

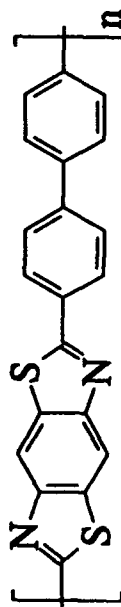
Figure 16. Decay dynamics of the photoinduced absorption maximum (680 nm) of a PBZT/TTA bilayer.

Figure 17. Time-resolved photoluminescence decay dynamics of : (1) PBO/TTA bilayer and (2) PBO thin film, both excited at 380 nm.

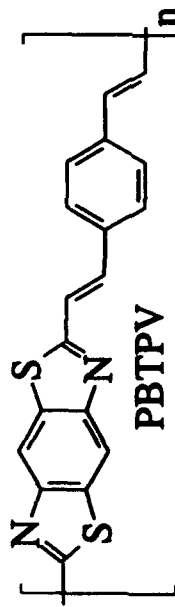
Chart I



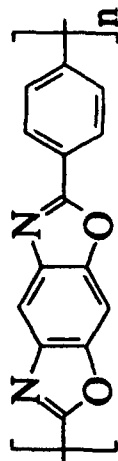
PBZT



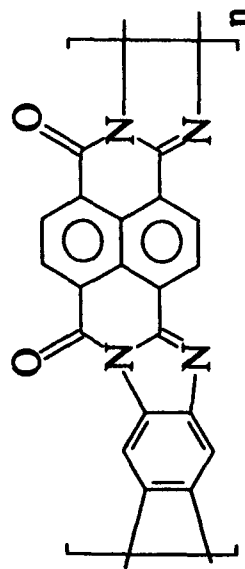
PBBZT



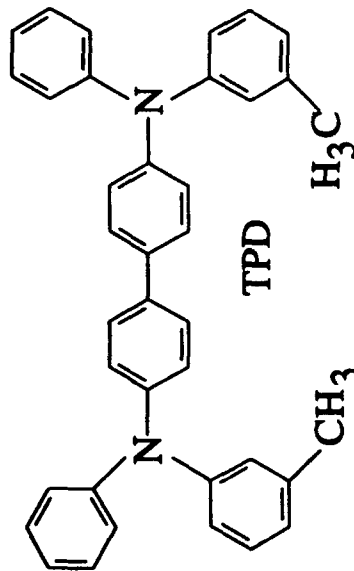
PBTPV



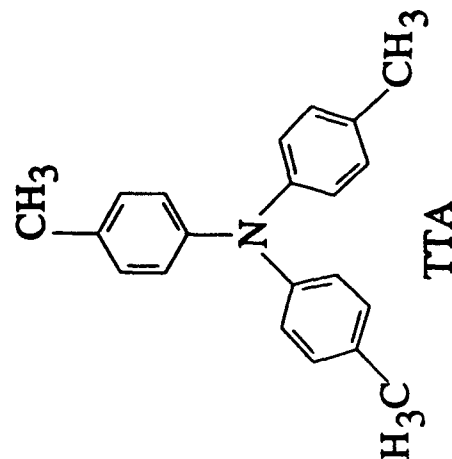
PBO



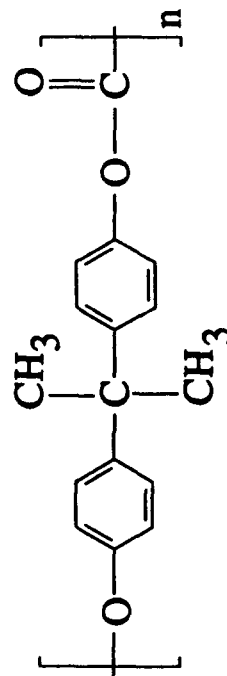
BBL



TPD



TTA



PC

Figure 1.

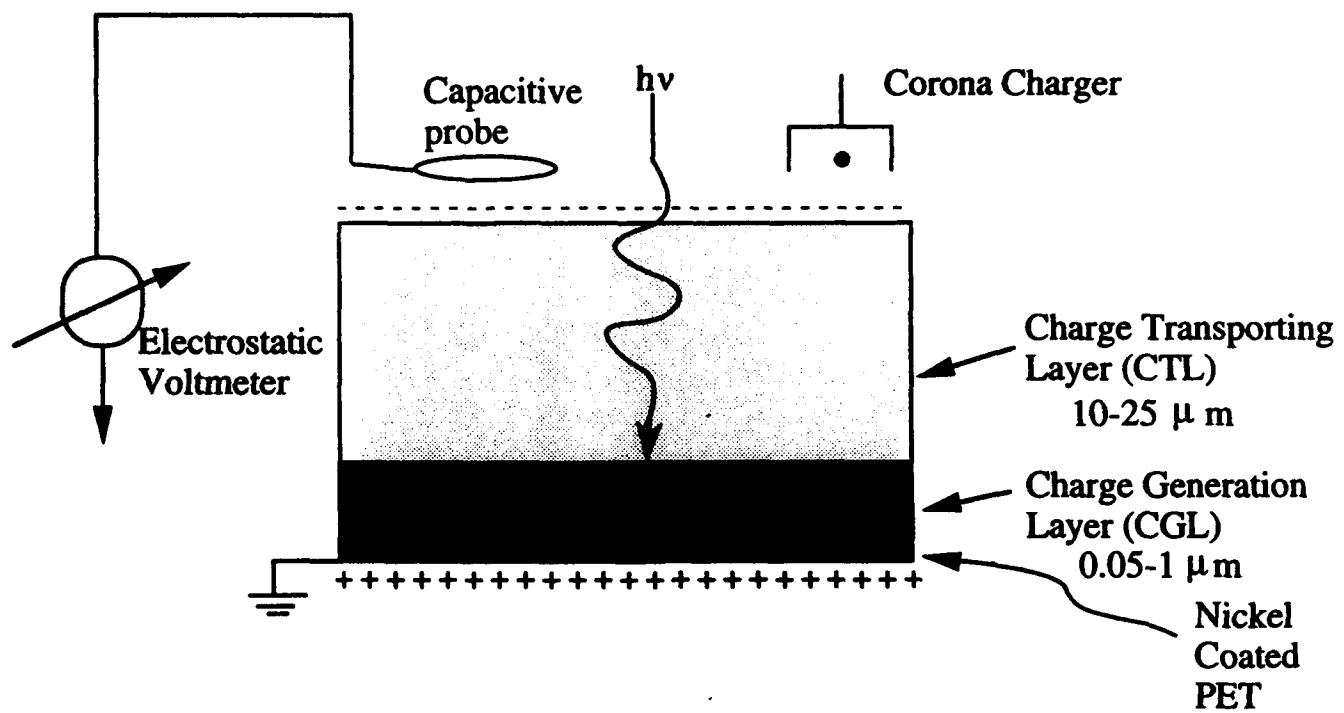


Figure 2

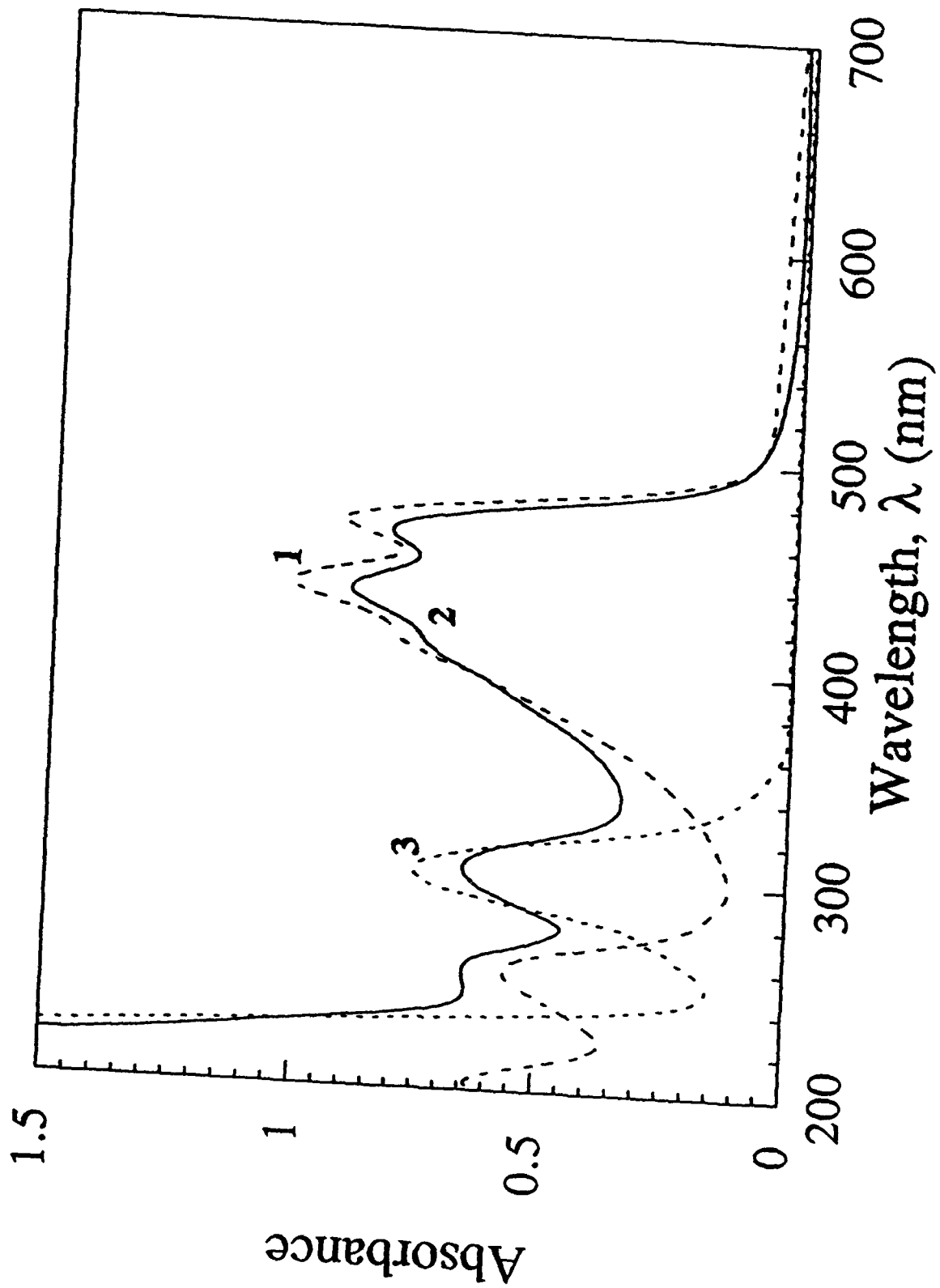


Figure 3

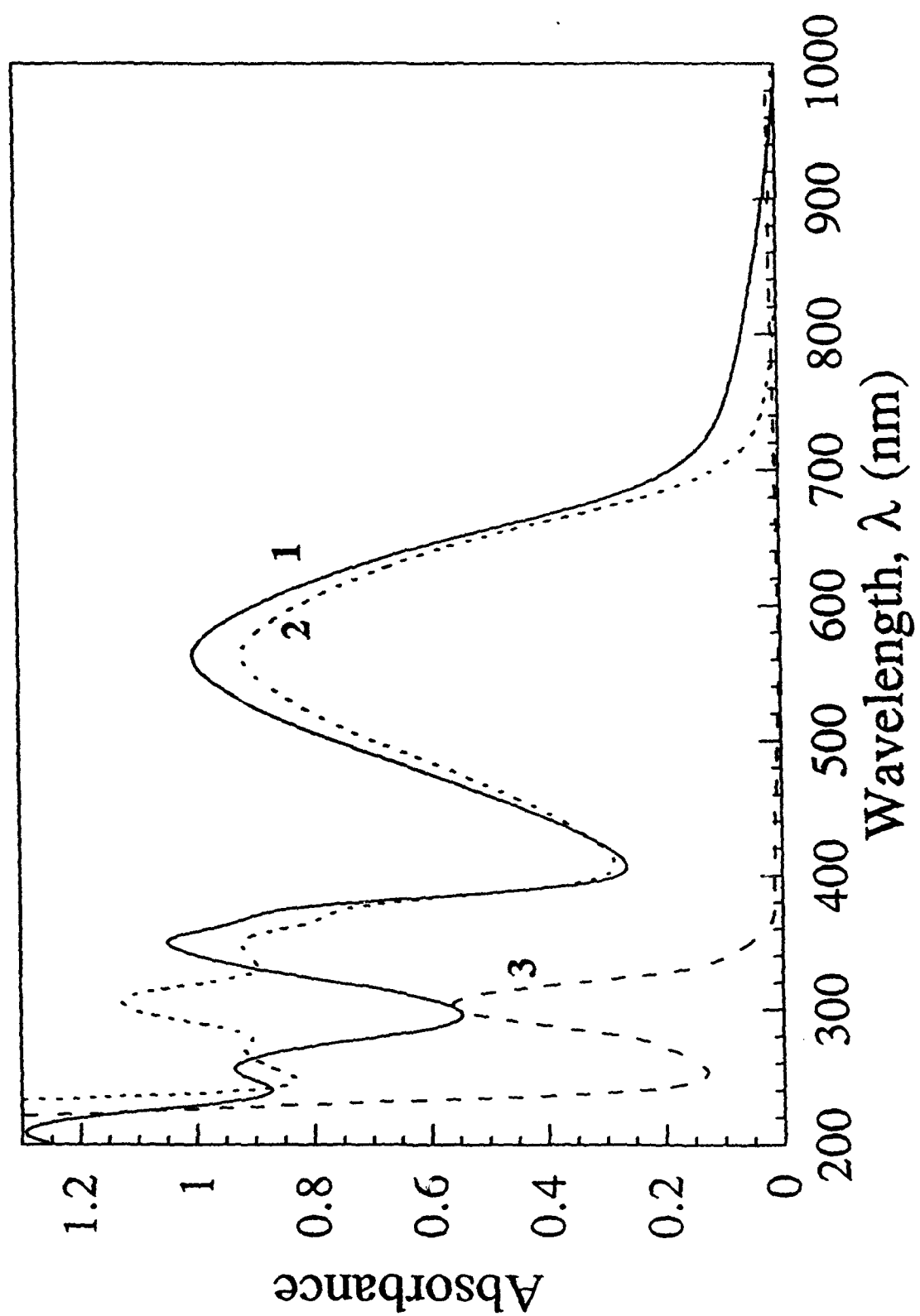


Figure 4

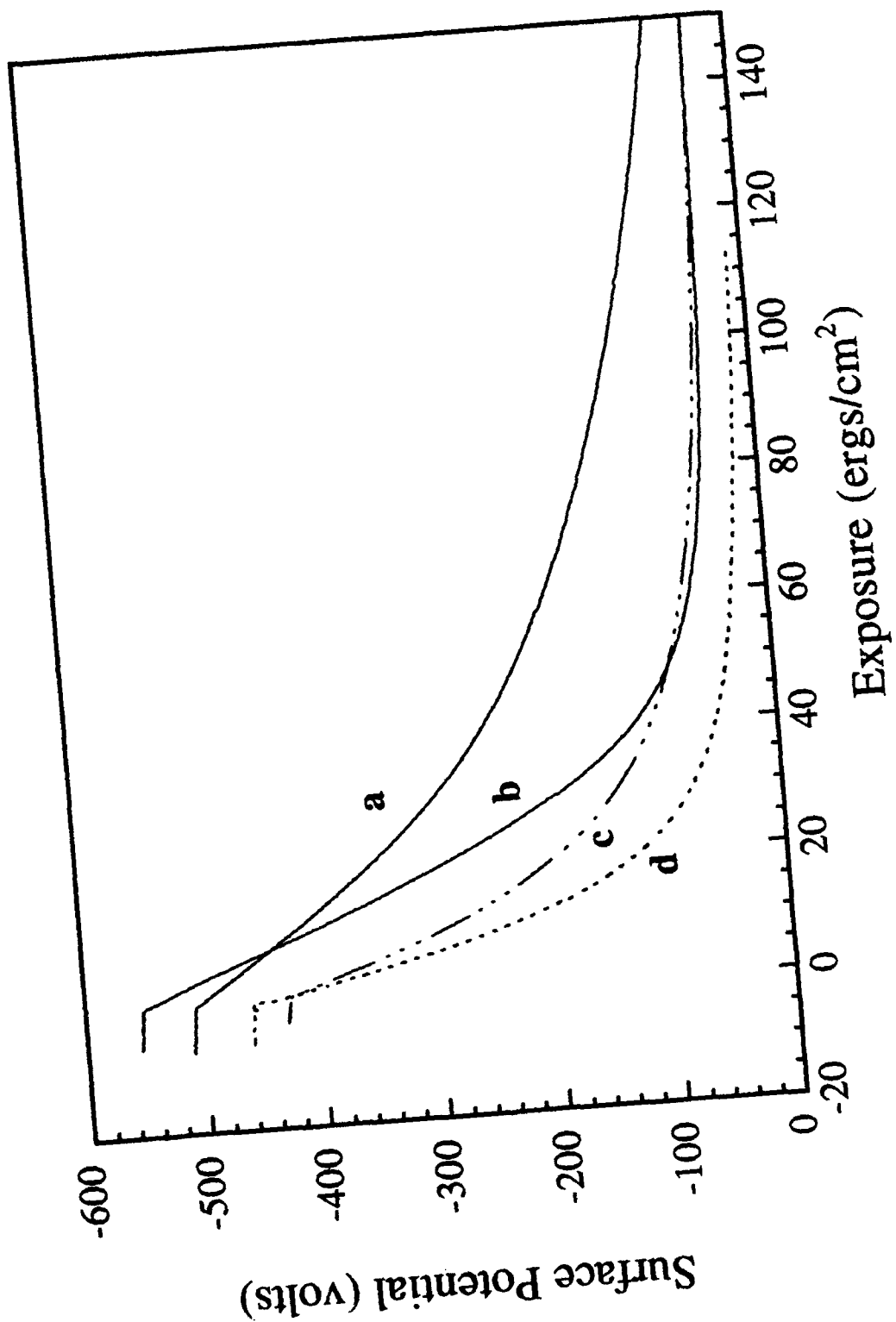


Figure 5

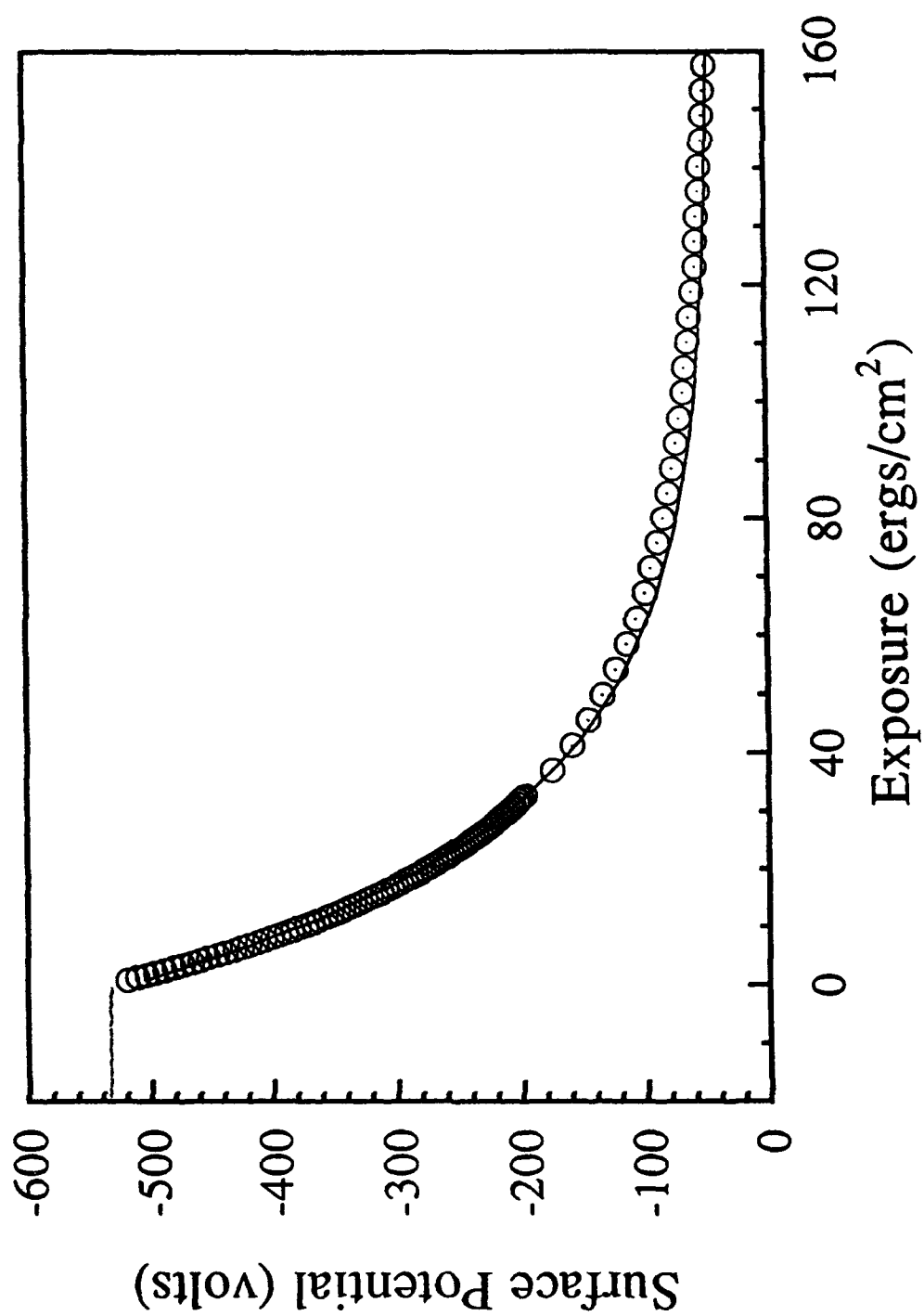
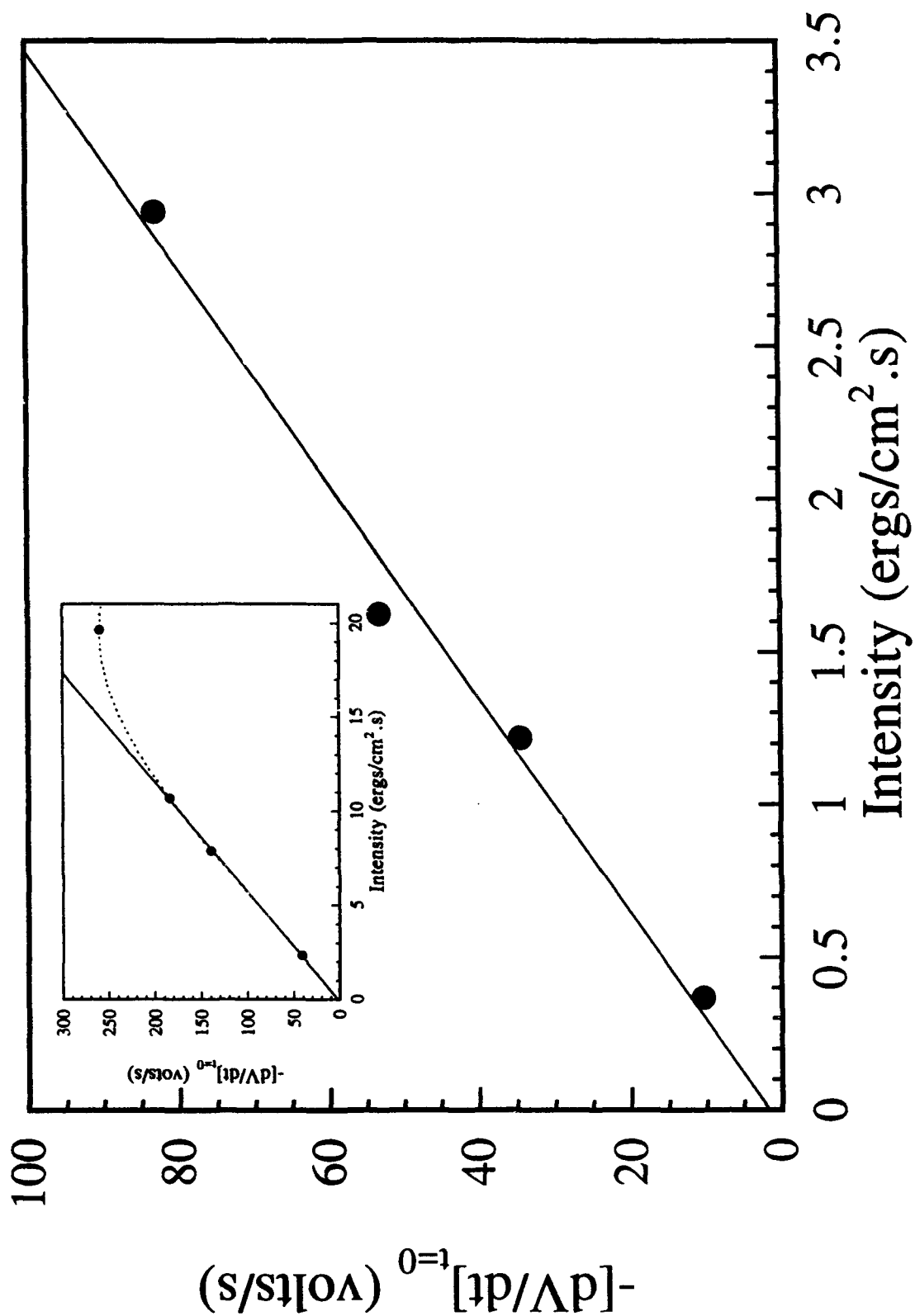


Figure 6



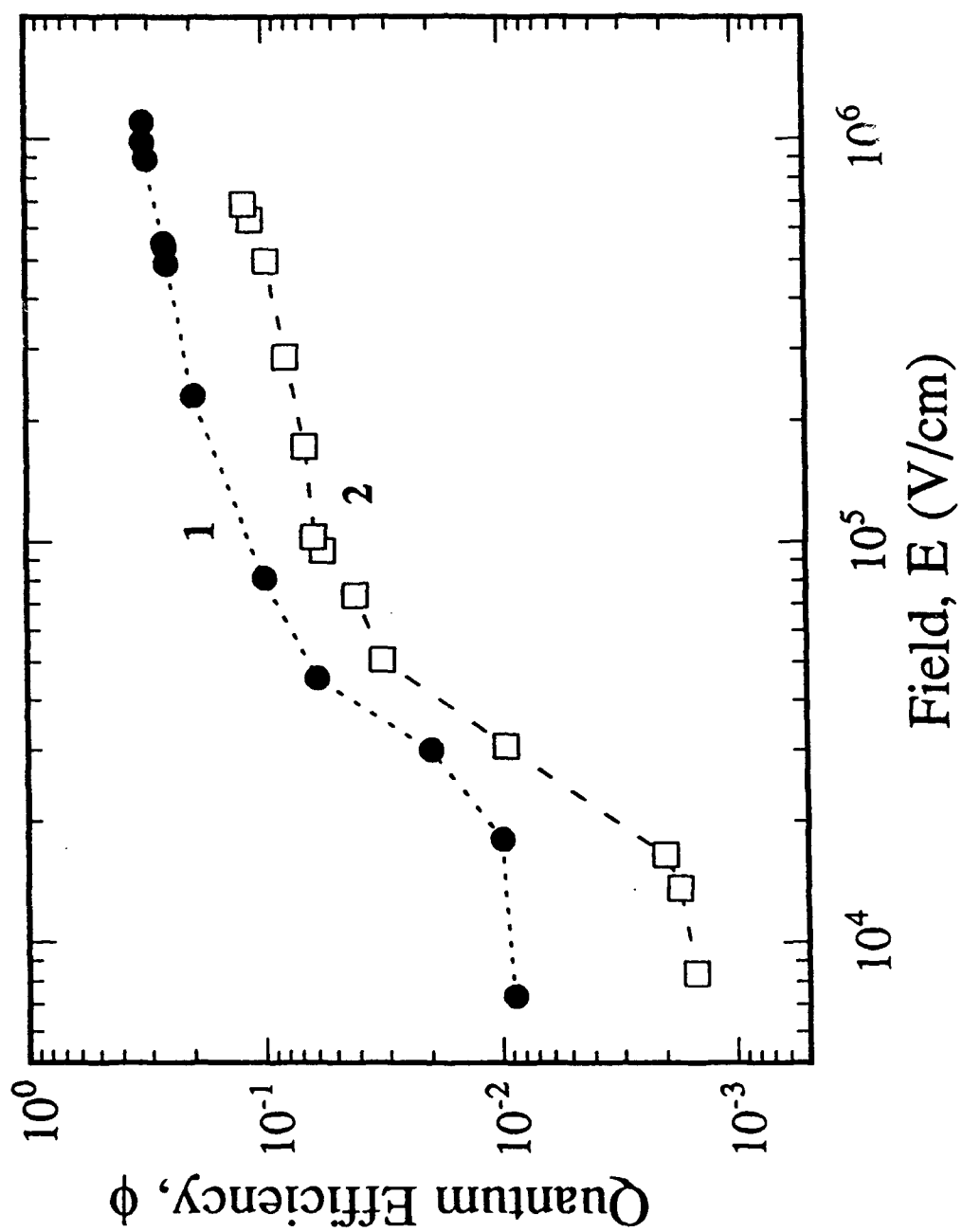


Figure 8

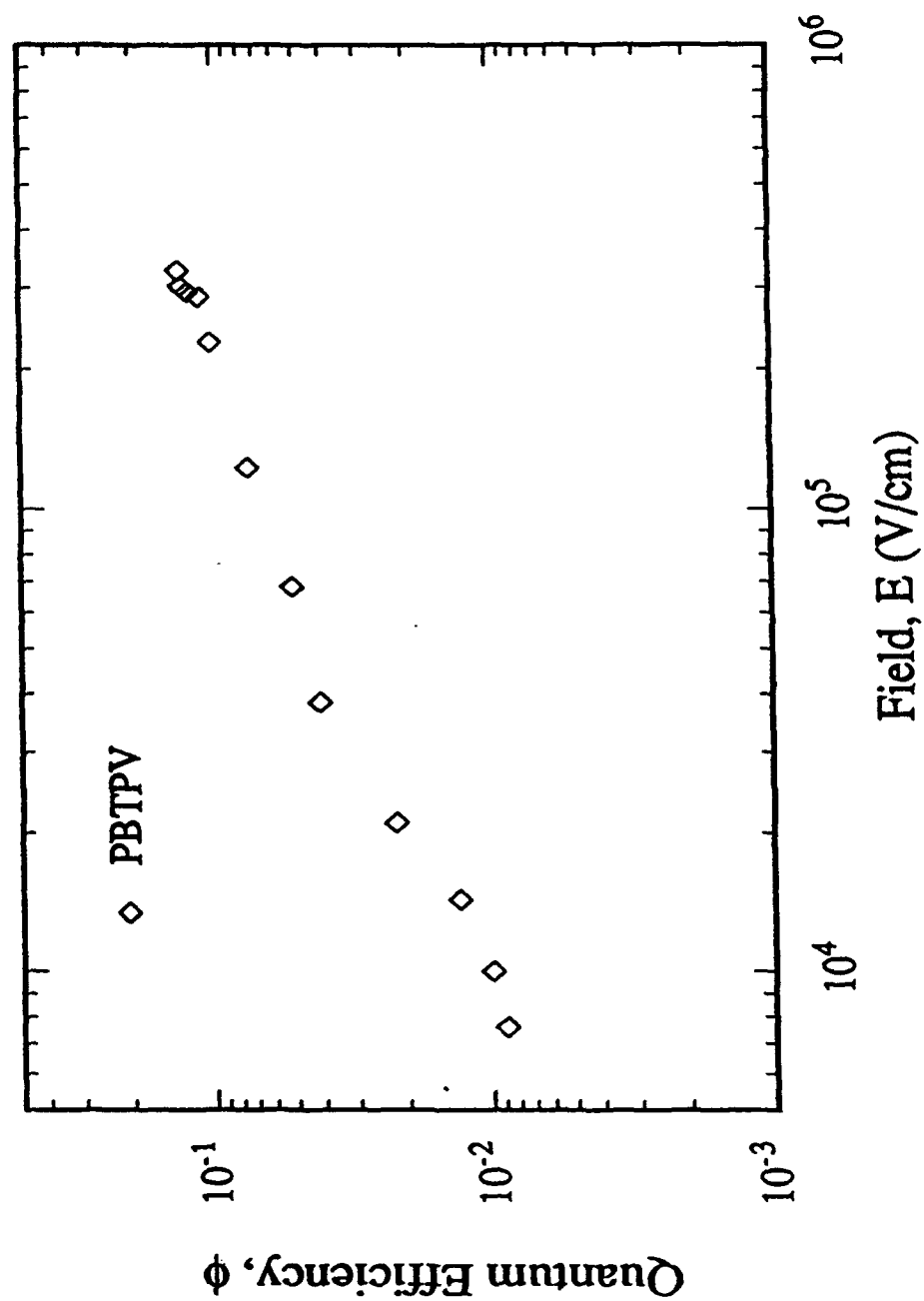


Figure 9

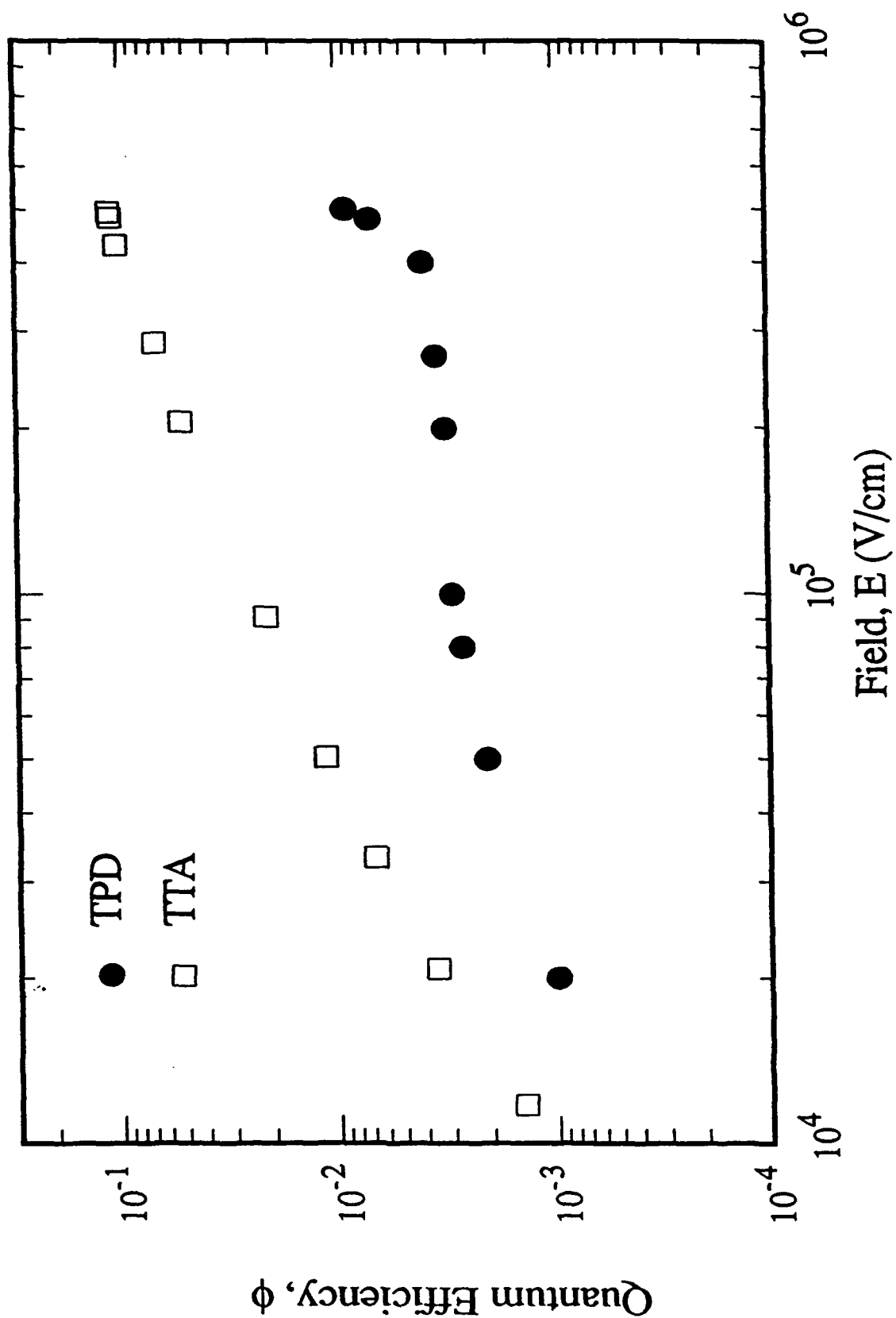


Figure 10

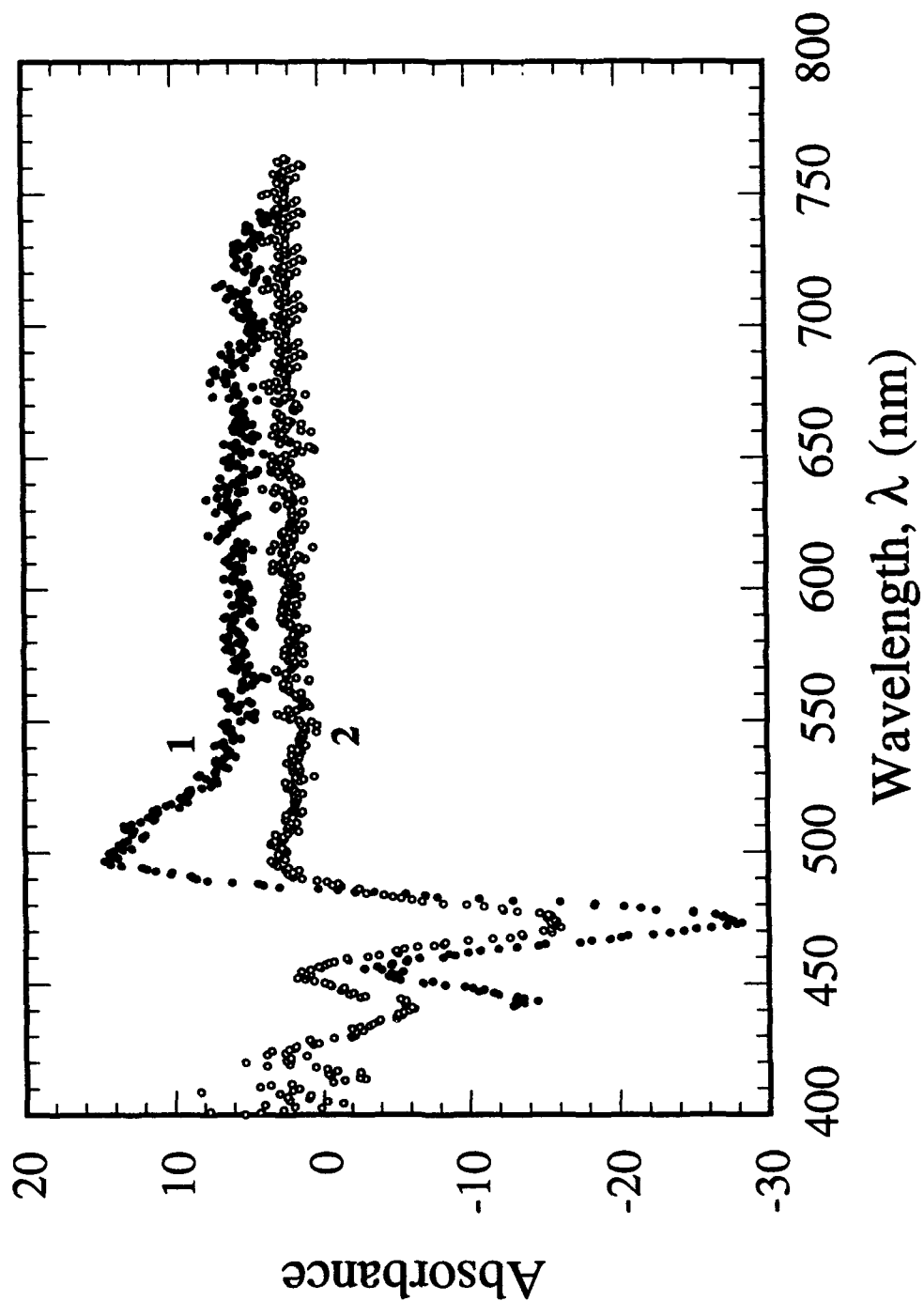


Figure 11

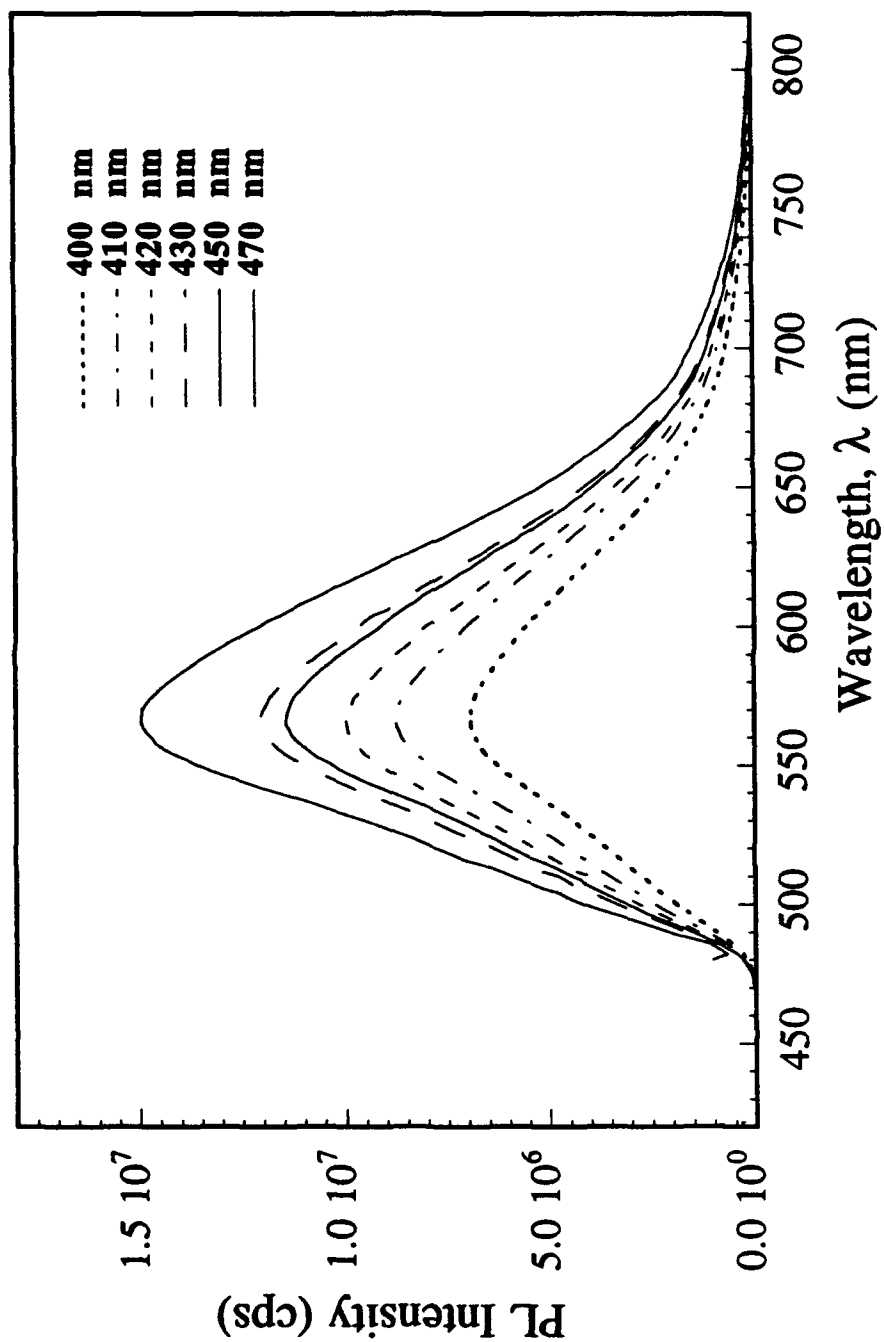


Figure 12

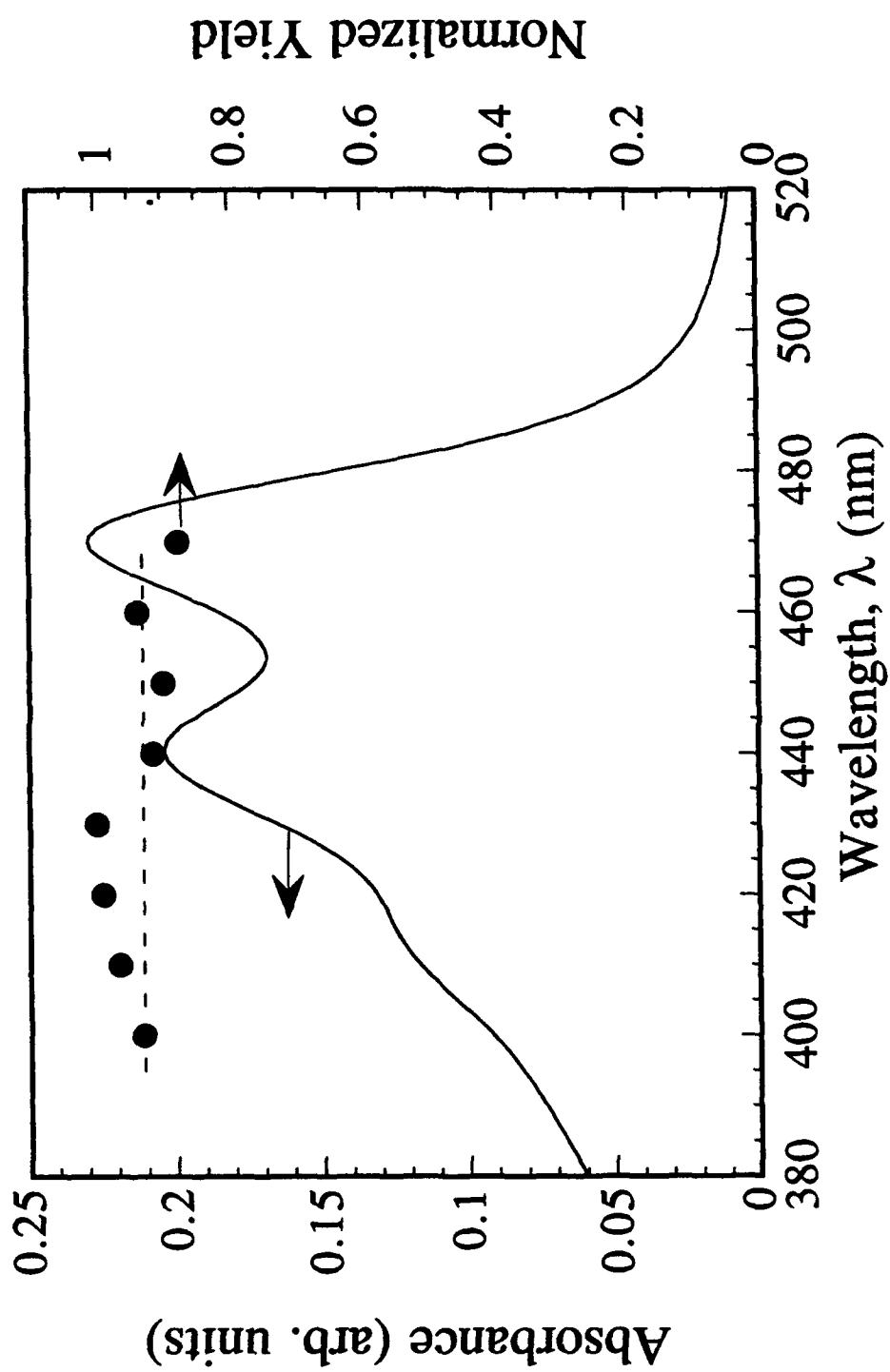


Figure 13

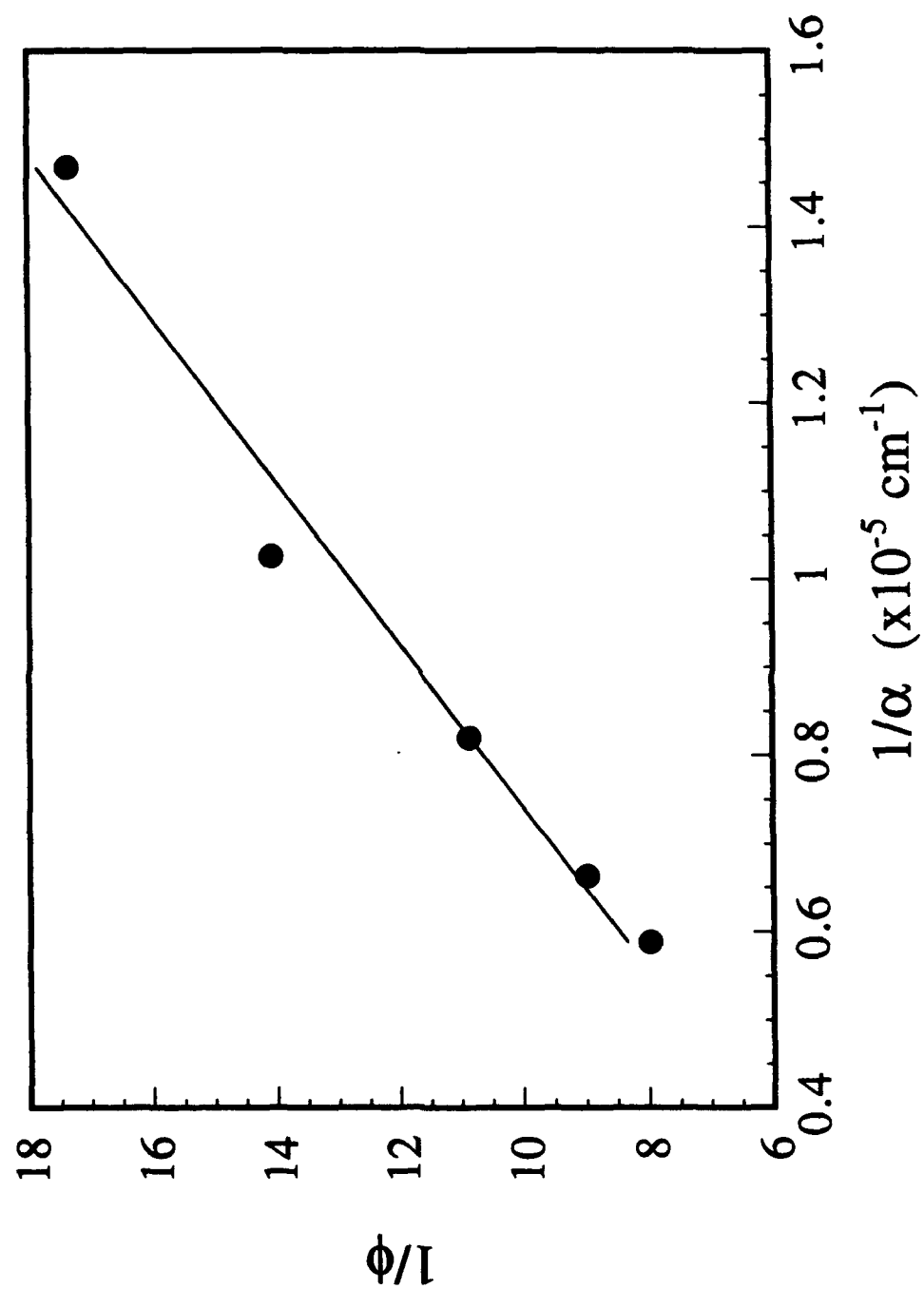


Figure 14

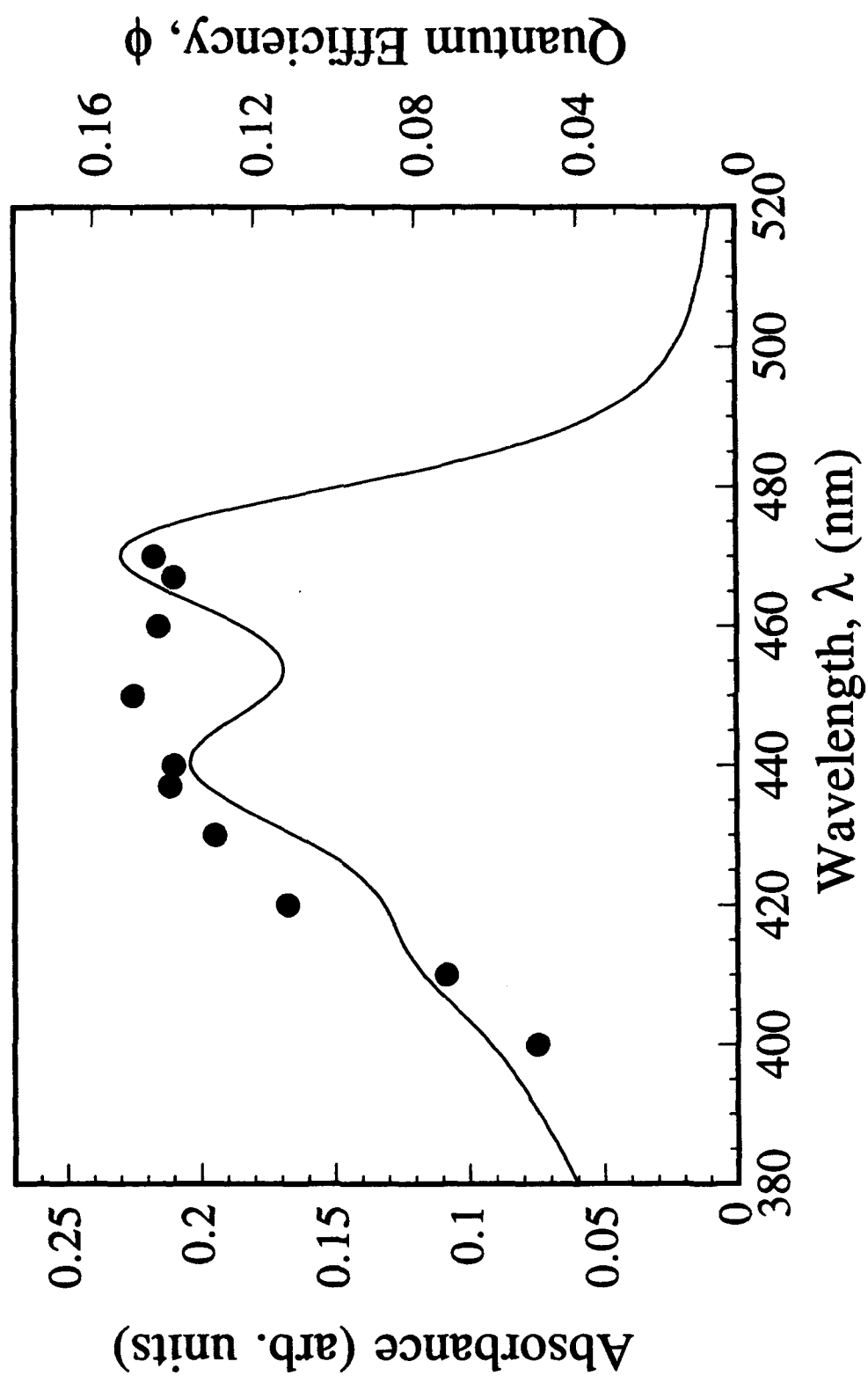


Figure 15

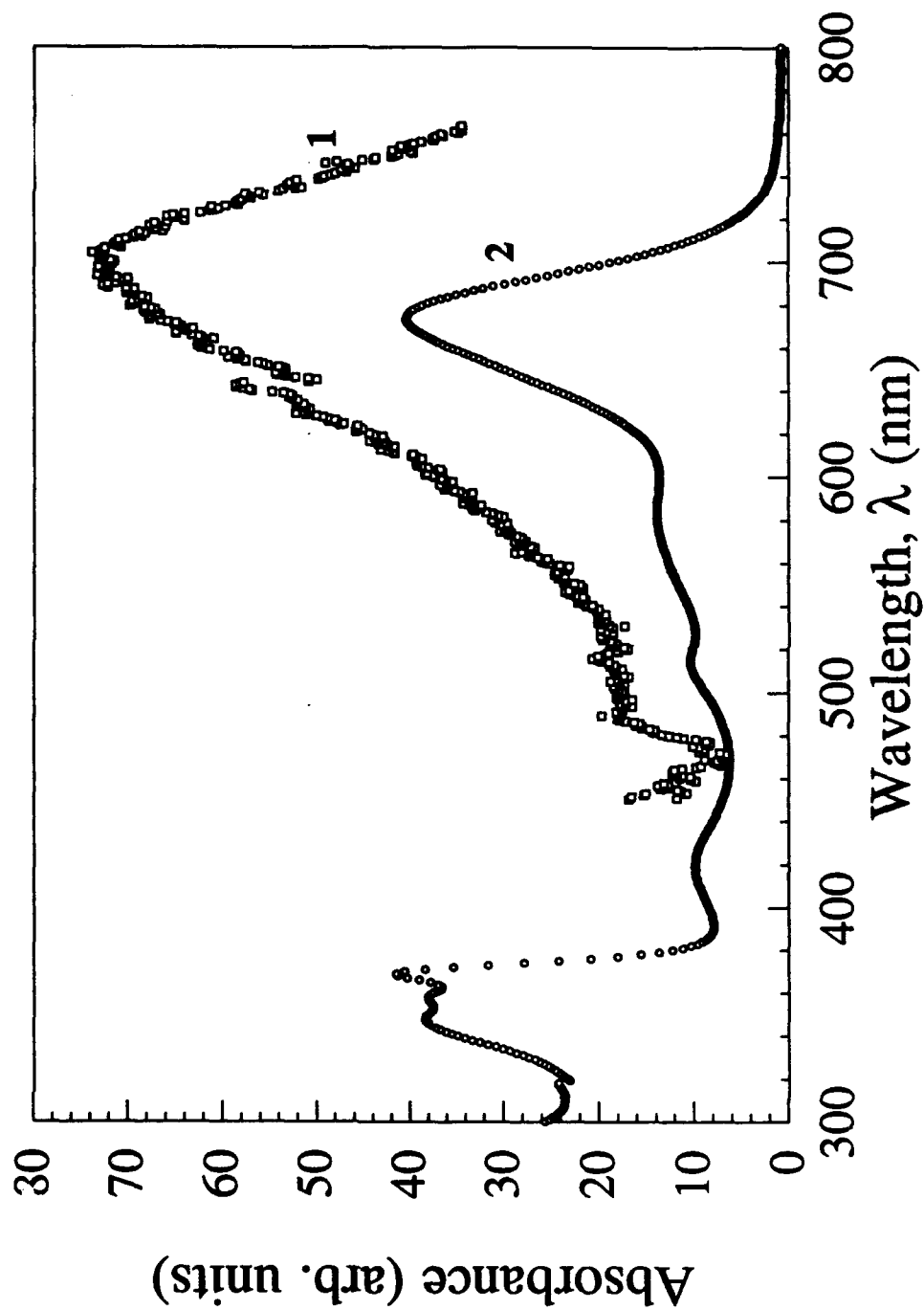


Figure 16

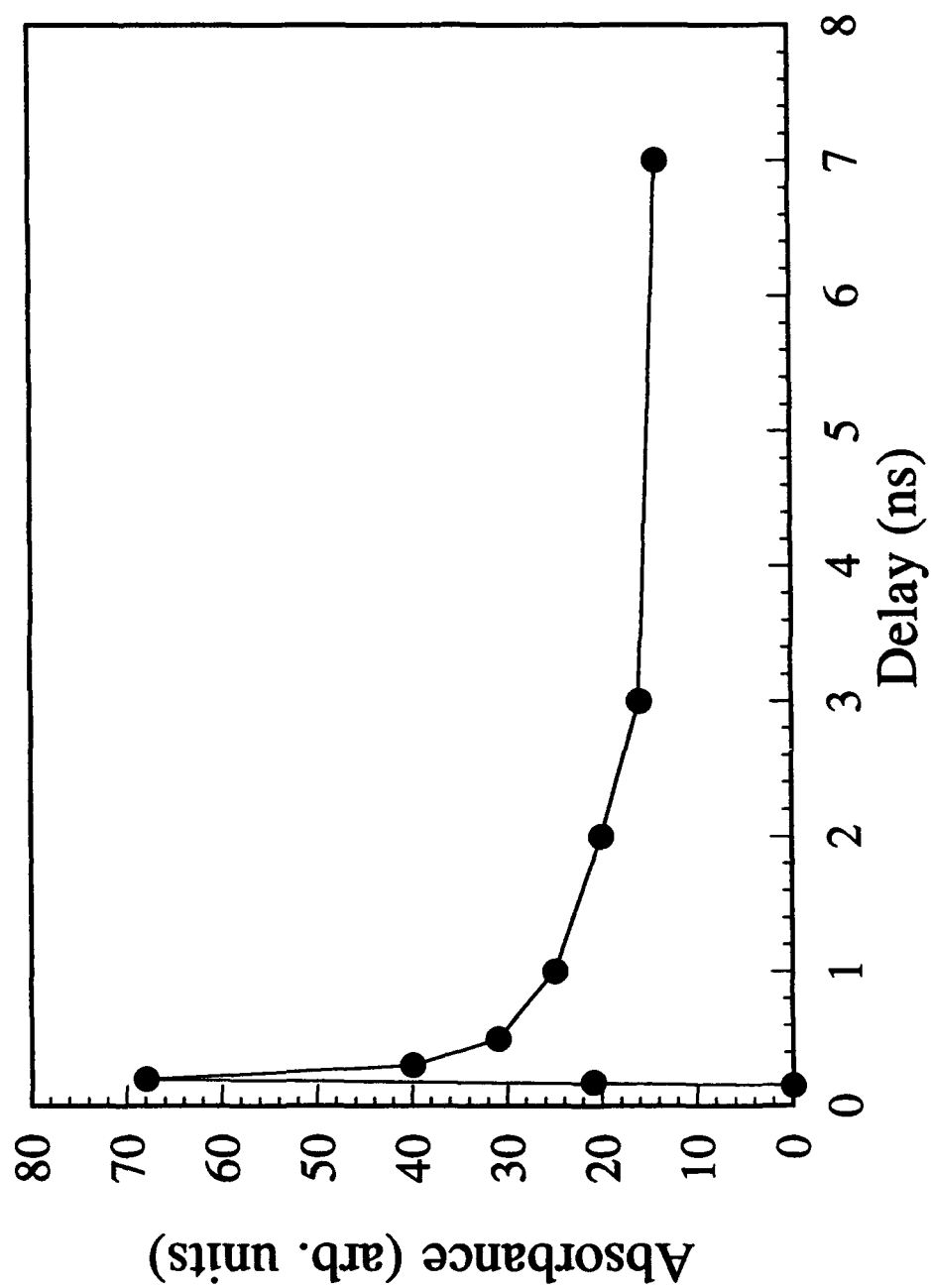


Figure 17

